Title: Neuropeptide Modulation Enables Biphasic Inter-network Coordination via a Dual-Network Neuron

Abbreviated Title: Biphasic Inter-network Coordination

Authors:
Barathan Gnanabharathi
Savanna-Rae H Fahoum
Dawn M Blitz

Affiliations:
Department of Biology
Center for Neuroscience and Behavior
Miami University
Oxford OH 45056

Contributions: S-RHF and DMB designed research, S-RHF and BG performed research, BG analyzed data, DMB and BG wrote the paper, DMB, S-RHF, and BG edited the paper

Correspondence should be addressed to
Dawn M. Blitz
700 E High St
PSN 212
Oxford OH, 45056
blitzdm@miamoh.edu
513-529-6327

Number of pages: 51
Number of figures: 8
Number of tables: 4
Number of words
- **Abstract**: 247
- **Significance Statement**: 118
- **Introduction**: 747
- **Discussion**: 2319

Acknowledgements: We thank Michael Hughes and Anh Vo (Statistical Consulting Center, Miami University) for assistance with statistical analysis.

Conflict of Interest:
The authors report no conflict of interest.

Funding sources: National Science Foundation IOS:1755283 (DMB), Biology Department, Miami University

Abstract

Linked rhythmic behaviors, such as respiration/locomotion or swallowing/chewing often require coordination for proper function. Despite its prevalence, the cellular mechanisms controlling coordination of the underlying neural networks remain undetermined in most systems. We use the stomatogastric nervous system of the crab *Cancer borealis* to investigate mechanisms of inter-network coordination, due to its small, well characterized feeding-related networks (gastric mill [chewing, ~0.1 Hz]; pyloric [filtering food, ~1 Hz]). Here, we investigate coordination between these networks during the Gly^1-SIFamide neuropeptide modulatory state. Gly^1-SIFamide activates a unique triphasic gastric mill rhythm in which the typically pyloric-only LPG neuron generates dual pyloric- plus gastric mill-timed oscillations. Additionally, the pyloric rhythm exhibits shorter cycles during gastric mill rhythm-timed LPG bursts, and longer cycles during IC, or IC plus LG gastric mill neuron bursts. Photoinactivation revealed that LPG is necessary to shorten pyloric cycle period, likely through its rectified electrical coupling to pyloric pacemaker neurons. Hyperpolarizing current injections demonstrated that although LG bursting enables IC bursts, only gastric mill rhythm bursts in IC are necessary to prolong the pyloric cycle period. Surprisingly, LPG photoinactivation also eliminated prolonged pyloric cycles, without changing IC firing frequency or gastric mill burst duration, suggesting that pyloric cycles are prolonged via IC synaptic inhibition of LPG, which indirectly slows the pyloric pacemakers via electrical coupling. Thus, the same dual-network neuron directly conveys excitation from its endogenous bursting and indirectly funnels synaptic inhibition to enable one network to alternately decrease and increase the cycle period of a related network.

Significance Statement

Related rhythmic behaviors frequently exhibit coordination, yet the cellular mechanisms coordinating the underlying neural networks are not determined in most systems. We investigated coordination between two small, well-characterized crustacean feeding-associated networks during a neuropeptide-elicited modulatory state. We find that a dual fast/slow network neuron directly shortens fast network cycles during its slow, intrinsically generated bursts, likely via electrical coupling to fast network pacemakers, despite rectification favoring the opposite direction. Additionally, the fast network is indirectly prolonged during another slow-network phase, via chemical synaptic inhibition that is likely funneled through the same electrical synapse. Thus, a dual-network neuron alternately reinforces and diminishes neuropeptide actions, enabling distinct frequencies of a faster network across different phases of a related slower rhythm.

Introduction

Many rhythmic behaviors require coordination for proper function, such as locomotion and respiration, and multiple orofacial behaviors (e.g., respiration, swallowing, chewing, vocalization) (Barnett et al., 2021; Cao et al., 2012; Hao et al., 2021; Huff et al., 2022; Juvin et al., 2022; Wei et al., 2022). Central pattern generator (CPG) networks controlling rhythmic behaviors are flexible to accommodate changing organismal needs (Bucher et al., 2015; Grillner and El Manira, 2020; Ramirez and Baertsch, 2018). Behavioral coordination requires coordinating the underlying CPG networks. Significant consequences occur from disrupted coordination, such as aspiration of food if swallowing and respiration are not coordinated (Yagi et al., 2017). Thus, it is important to understand the cellular-level mechanisms controlling inter-network coordination.

Network coordination can occur as correlated changes in frequency or strength, as for respiration with changing locomotor speeds or at the onset of vocalizations, or as specific timing relationships to coordinate movements of different body parts (Anderson et al., 2016; Daley et al., 2013; Demartsev et al., 2022; Juvin et al., 2022; Mulloney and Smarandache-Wellmann, 2012; Ramirez and Baertsch, 2018; Wei et al., 2022). Such interactions may occur via direct CPG to CPG projections, or indirectly via feedback from networks to higher-order inputs to a related CPG (Bartos and Nusbaum, 1997; Gariépy et al., 2010; Wood et al., 2004). Additional anatomical substrates for network coordination include sensory feedback from one behavior influencing related CPGs, or parallel descending input to related networks (Barnett et al., 2021; Gariépy et al., 2010; Juvin et al., 2022). More complex behavioral interactions may also occur, such as

variations in respiration during crying, singing, or while playing wind instruments (Fortune et al., 2011; Hérent et al., 2023; Higashino et al., 2022; Okobi et al., 2019; Wei et al., 2022). Further, coordination can be altered by developmental, physiological, or environmental stimuli (Blitz and Nusbaum, 2008; Clemens et al., 1998a; Moore et al., 2013; Saunders et al., 2004; Sillar et al., 2023; Stein and Harzsch, 2021). Although insights have been gained into inter-network coordination, its complexity and plasticity coupled with often large, distributed networks make it difficult to fully determine how network coordination is controlled (Juvin et al., 2022).

Here we used small, well-described networks in the stomatogastric nervous system (STNS) of the Jonah crab, *Cancer borealis*, to investigate cellular-level mechanisms of inter-network coordination (Bartos et al., 1999; Bartos and Nusbaum, 1997; Daur et al., 2016; Wood et al., 2004). An in vitro STNS preparation includes the stomatogastric ganglion (STG, ~30 neurons) containing well-characterized CPGs that control the gastric mill (food chewing) and pyloric (food filtering) rhythms, plus identified modulatory and sensory inputs (Fig. 1) (Blitz, 2023; Daur et al., 2016; Nusbaum and Beenhakker, 2002). The pacemaker-driven pyloric rhythm is constitutively active in vivo and in vitro (~1 s cycle period), whereas the slower (~10 s cycle period) network-driven gastric mill CPG requires activation by modulatory or sensory inputs (Blitz, 2023; Nusbaum and Beenhakker, 2002). All pyloric and gastric mill neurons (1-5 neurons/type) and their transmitters are identified, and their connectivity is mapped under multiple modulatory conditions (Fig. 1B) (Daur et al., 2016; Fahoum and Blitz, 2024; Marder and Bucher, 2007). Although the gastric mill and pyloric rhythms can occur independently, they are often coordinated, and the extent and type of coordination

129 is altered by modulatory, behavioral, and environmental conditions (Bartos et al., 1999;
130 Bartos and Nusbaum, 1997; Blitz et al., 2019; Clemens et al., 1998a; Stein and
131 Harzsch, 2021; Wood et al., 2004).

132 We investigated mechanisms of coordination during the modulatory state elicited
133 by the modulatory commissural neuron 5 (MCN5), or bath application of its
134 neuropeptide Gly^1-SIFamide (Blitz et al., 2019; Fahoum and Blitz, 2021; Fahoum and
135 Blitz, 2024). In this state, the typically pyloric-only LPG switches into dual pyloric and
136 gastric mill rhythm participation, becoming the third phase of a gastric mill rhythm
137 (Fahoum and Blitz, 2024). This contrasts with biphasic gastric mill rhythm versions
138 (Beenhakker et al., 2004; Blitz et al., 2008, 1999; Christie et al., 2004). The pyloric
139 rhythm cycle period varies across the Gly^1-SIFamide gastric mill rhythm, but a full
140 description plus identification of mechanisms of interactions between the two networks
141 is lacking (Blitz et al., 2019). The well-described connectome and small populations
142 enabled selective manipulation of neuronal populations to determine the full extent of
143 gastric mill regulation of the pyloric rhythm and its underlying cellular mechanisms
144 during the unique triphasic Gly^1-SIFamide-elicited gastric mill rhythm. Our results
145 highlight the complexity of synaptic connectivity that can mediate coordination between
146 related networks.

147 **Methods**

148 **Animals**

149 Wild caught adult male *C. borealis* crabs were procured from The Fresh Lobster
150 Company (Gloucester, MA), maintained in artificial seawater (10-12°C) tanks, and fed
151 twice weekly until used. Prior to dissection, crabs were anesthetized by cold packing in

152 ice for 40 – 50 minutes. The crab foregut was first removed, bisected, and pinned flat,
153 ventral side up, in a Sylgard 170-lined dish (Thermo Fisher Scientific). The STNS was
154 then dissected free from muscles and connective tissue and pinned in a Sylgard 184-
155 lined petri dish (Thermo Fisher Scientific) (Fahoum and Blitz, 2021; Gutierrez and
156 Grashow, 2009). The preparation was kept in chilled (4°C) *C. borealis* physiological
157 saline throughout dissections.

158

159 **Solutions**

160 *C. borealis* physiological saline was composed of 440 mM NaCl, 26 mM $MgCl_2$,
161 13 mM $CaCl_2$, 11 mM KCl, 10 mM Trizma base, 5 mM maleic acid (pH 7.4-7.6). Squid
162 internal electrode solution contained 10 mM $MgCl_2$, 400 mM potassium D-gluconic acid,
163 10 mM HEPES, 15 mM Na_2SO_4, 20 mM NaCl, pH 7.45 (Hooper et al., 2015). Gly^1-
164 SIFamide (GYRKPPFNG-SIFamide, custom peptide synthesis: Genscript) (Blitz et al.,
165 2019; Dickinson et al., 2008; Huybrechts et al., 2003; Yasuda et al., 2004) was
166 prepared by dissolving it in optima water (Thermo Fisher Scientific) at 10 mM, and
167 aliquoting and storing it at -20°C. Aliquots were diluted in physiological saline to a final
168 concentration of 5 μM before use in experiments.

169 **Electrophysiology**

170 The STNS preparation was superfused continuously with chilled *C. borealis*
171 physiological saline (8 - 10°C), or Gly^1-SIFamide (5 μM) diluted in saline. A switching
172 manifold enabled uninterrupted superfusion of the STNS preparation during solution
173 changes. Extracellular activity was recorded from nerves with custom stainless-steel pin
174 electrodes and a model 1700 A-M Systems Amplifier. The stomatogastric ganglion

175 (STG) was desheathed to gain access for intracellular recording of STG somata. Light
176 transmitted through a dark field condenser (MBL-12010 Nikon Instruments) provided
177 visualization of STG neuron somata. For intracellular recordings of STG neurons, sharp-
178 tip glass microelectrodes pulled using a glass electrode puller (P-97, Flaming/Brown
179 microelectrode puller, Sutter Instrument Co.) were used. Microelectrodes were filled
180 with a squid internal solution (see Solutions) (resistance: 20 – 40 MΩ) (Hooper et al.,
181 2015). Axoclamp 900A amplifiers (Molecular Devices) were used to collect intracellular
182 recordings in current clamp mode. Recordings were collected before, during, and after
183 the transection of both inferior and superior oesophageal nerves (*ion* and *son,*
184 respectively), to isolate the STG from descending neuromodulatory inputs. Data
185 presented were collected after transections were performed, unless otherwise noted.
186 For intracellular recordings, STG neuronal cell bodies were identified using extracellular
187 nerve recordings and/or their interactions with other STG neurons. All recordings were
188 collected using acquisition hardware (Micro1401; Cambridge Electronic Design) and
189 software (Spike2 Version 8.02e; ~5kHz sampling rate; Cambridge Electronic Design)
190 and a laboratory computer (Dell).

191 A data set from Fahoum and Blitz (2021) was re-used in this study for different
192 measurements than the previous study. As described, activity in the inferior cardiac (IC),
193 lateral gastric (LG), or dorsal gastric (DG) neurons, or all three neurons simultaneously,
194 was eliminated via hyperpolarizing current injection (-2 to -4 nA). Neurons were
195 hyperpolarized sufficiently to eliminate spike-mediated and graded transmitter release
196 (Fahoum and Blitz, 2021).

197 For the established biological model of MCN5 actions, it is necessary to eliminate
198 LP activity to mimic the MCN1 glutamatergic inhibition of LP (Fahoum and Blitz, 2021).
199 Therefore, for all experiments using bath-application of Gly^1-SIFamide (5 μM), the
200 lateral pyloric (LP) neuron was either hyperpolarized (-2 to -4 nA) or photoinactivated
201 (Fahoum and Blitz, 2021; Snyder and Blitz, 2022). To selectively eliminate the influence
202 of the single LP neuron or the two copies of the LPG neurons, neurons were impaled
203 with a microelectrode that was tip-filled with AlexaFluor-568 hydrazide (10 mM in 200
204 mM KCl; Thermo Fisher Scientific) and backfilled with squid internal solution. The
205 neurons were injected with -5 nA hyperpolarizing current (for either ~ 30 min, or for 5 to
206 10 min and the dye then allowed to diffuse for an additional ~30 min) to fill their soma
207 and neurites with the AlexaFluor-568 dye. The STG was then illuminated with a Texas
208 red filter set (560 ± 40 nm wavelength; Leica Microsystems, 3-7 min). The neurons were
209 considered completely photoinactivated when the membrane potential reached 0 mV,
210 and their action potentials were absent in either the lateral ventricular nerve (*lvn;* for LP)
211 or the lateral posterior gastric nerve (*lpgn;* for LPG).

212

213 **Data analysis**

214 **Neuronal Activity Quantification**

215 The number of bursts, burst duration (s), cycle period (s; start of one burst to the
216 start of the subsequent burst of a reference neuron), number of spikes per burst, and
217 firing frequency (Hz; [number of spikes per burst – 1]/burst duration) were quantified
218 using a custom Spike2 script. Each activity parameter was averaged across 20 min,
219 unless otherwise noted. All analyses were performed after the effects of Gly^1-SIFamide

application reached steady state. Steady state was noted when LPG elicited consistent dual-network bursting (e.g., Fig. 1Ciii) with consistent gastric mill-timed bursting of LG, IC, and DG (~ 10 min from the start of Gly^1-SIFamide bath application). The pyloric cycle period was quantified as the duration(s) from the start of one pyloric dilator (PD) neuron burst to the start of the subsequent PD burst (Bartos et al., 1999). In the Saline:*ions*/*sons* cut condition, in which the *ions/sons* were transected, the pyloric cycle period did not always express a full triphasic pattern, due to the lack of modulatory input (Hamood et al., 2015; Spencer and Blitz, 2016; Zhang et al., 2009). However, when this occurred, the pyloric rhythm returned during the Gly^1-SIFamide bath application. A Saline:*ions/sons* cut condition was excluded from analysis if PD neuron bursting was intermittently active, was completely absent, or if the PD neurons were rhythmically active but had ≤ 2 action potentials per burst. Pyloric cycle periods were measured across the final 20 min of 30 min Gly^1-SIFamide (5 μM) bath applications, and across 200 s windows for Saline:Intact STNS and the Saline:*ion/son* cut conditions.

Gastric mill-timed IC bursts were identified as those that had burst durations greater than 0.45 s (Blitz et al., 2019; Fahoum and Blitz, 2024). Multiple IC bursts with greater than 0.45 s burst durations, were grouped into a single “gastric mill” burst if the distance between each burst was less than 2 s, otherwise they were considered as individual bursts. If there was an IC burst with a burst duration less than 0.45 s between two gastric mill IC bursts that were less than 2 s apart, they were grouped together as one gastric mill burst. Within an IC gastric mill-timed burst, pyloric-timed IC bursts were identified if there was an interruption timed to a PD burst (e.g., Fig. 6Ai-ii). We identified LPG gastric mill-timed bursts (LPG slow bursts) as previously described (Fahoum and

243 Blitz, 2021; Fahoum and Blitz, 2024; Snyder and Blitz, 2022). Briefly, from a histogram
244 of all LPG inter-spike intervals (ISIs) made in Excel (Microsoft), peaks of intraburst
245 (interval between spikes during a burst) and interburst (interval between spikes between
246 burst) intervals were identified. The mean ISI was calculated between these two peaks
247 and used to identify LPG bursts. A custom written Spike2 script was then used to
248 identify LPG gastric mill-timed slow bursts and exclude pyloric-timed LPG bursts using
249 PD activity as a reference (Fahoum and Blitz, 2021). Coefficient of variation (CV) of
250 pyloric cycle periods was calculated as Standard Deviation / Mean.
251

252 **Analysis of pyloric cycle period relative to gastric mill neuron activity**

253 To analyze pyloric cycle periods based on which gastric mill neurons were active,
254 burst timings for each neuron over a 20 min window, unless otherwise indicated, were
255 exported from Spike2 to MATLAB (MathWorks) for further analysis. A custom written
256 MATLAB script categorized PD cycle periods according to which gastric mill neuron(s)
257 bursts overlapped with each pyloric cycle. This included any amount of overlap between
258 a pyloric cycle period and a gastric mill neuron burst. Pyloric cycle periods that did not
259 overlap with any gastric mill neurons were placed into the SIFbaseline category, i.e., no
260 gastric mill neurons active. Pyloric cycle periods assigned to a particular category were
261 averaged for each preparation, and a total average was then calculated across all
262 experiments for each category. In some preparations, no pyloric cycle periods were
263 assigned to some of the categories. Specifically, for IC, LPG:IC, and LPG:DG:IC there
264 were 9 to 10 preparations that had no cycle periods assigned to each of these
265 categories while for the remaining 13 categories there were 0 to 3 preparations that had

no pyloric cycles assigned to these categories. This data set (n=16/19 from Fahoum and Blitz, 2021) and the LPG:Intact and LPG:Kill condition experiments (n=9/9 from Fahoum and Blitz, 2024) were reanalyzed from previous studies. Two experiments from the original data set of 11 were excluded from analysis due to a lack of biphasic regulation in the LPG:Intact condition.

Due to the inter-preparation variability of the pyloric cycle period, to test for changes in regulation of the pyloric cycle period between LPG:Kill and LPG:Intact conditions, all pyloric cycle periods were normalized to the average pyloric cycle period in the SIFbaseline category in each experiment. All pyloric cycle periods after normalization were plotted as a histogram with a bin size of 3 ms for both conditions. Further, bin counts for each histogram were normalized to the peak count in that condition to compare the overall distribution of the two histograms. Normalization and histogram plotting were performed using a custom written MATLAB script.

Figure preparation and statistical analysis

Burst and spike identification from raw data was performed with custom-written scripts in Spike2, and exported to either Microsoft Excel or MATLAB for further analysis. Pyloric cycle period histograms were plotted using a script written in MATLAB. Figures were created using graphs and recordings exported from MATLAB, SigmaPlot (Systat, v13), and Spike2 into CorelDraw (Corel, v24). Statistical analyses were performed using SigmaPlot software and R statistical software (v4.1.1). Data were analyzed for normality using the Shapiro-Wilk test to determine whether a non-parametric or parametric test would be used. Paired *t* test, One Way Repeated Measures ANOVA, mixed model

289 ANOVA, and *post hoc tests* were used as noted. For all tests, we used an alpha level of
290 0.05. Data are presented as mean ± SE.

291

292 **Code accessibility**

293 Spike2 and MATLAB scripts used for analysis are available at
294 https://github.com/blitzdm/GnanabharathiFahoumBlitz2024.

295

296 **Results**

297 **Gly^1-SIFamide elicits a variable pyloric rhythm**

298 The modulatory projection neuron MCN5 elicits a unique gastric mill rhythm that
299 can be reproduced in vitro by bath application of the MCN5 neuropeptide Gly^1-SIFamide
300 plus elimination of LP neuron activity (Blitz et al., 2019; Fahoum and Blitz, 2021;
301 Fahoum and Blitz, 2024). MCN5 inhibits LP via its cotransmitter glutamate, but Gly^1-
302 SIFamide bath application excites LP, likely mimicking the actions of a second Gly^1-
303 SIFamide-containing input to the STG (Blitz et al., 2019; Fahoum and Blitz, 2021).
304 Therefore, we hyperpolarized or photoinactivated the LP neuron to enable LPG dual-
305 network activity and better mimic the MCN5-elicited motor pattern. In *C. borealis*, LPG is
306 typically only active with the pyloric network due to its electrical coupling with the rest of
307 the pyloric pacemaker ensemble (Fig. 1B-C) (Shruti et al., 2014), but switches into dual-
308 network activity characterized by longer-duration, slower gastric mill-timed bursts
309 alternating with shorter duration, faster pyloric-timed bursts during Gly^1-SIFamide
310 application (Fig. 1Ciii) (Blitz et al., 2019; Fahoum and Blitz, 2021; Fahoum and Blitz,

311 2024). The unique Gly^1-SIFamide gastric mill rhythm is characterized by co-activity of
312 LG and IC neurons that are primarily out of phase with DG neuron activity, followed by
313 LPG neuron gastric mill activity (Blitz et al., 2019; Fahoum and Blitz, 2024) (Fig. 1C).
314 Anecdotally, the pyloric rhythm cycle period varies throughout the Gly^1-SIFamide gastric
315 mill rhythm, with a correlation between IC burst duration and extended duration pyloric
316 cycles (Blitz et al., 2019; Fahoum and Blitz, 2021). Here we investigate in detail the
317 timing relationship between pyloric and gastric mill rhythms in the Gly^1-SIFamide
318 modulatory state.

319 We first quantified the variability of the pyloric rhythm by measuring the
320 coefficient of variation (CV) in control and during the Gly^1-SIFamide gastric mill rhythm.
321 To eliminate confounds due to a potentially variable set of endogenously active
322 modulatory inputs, we transected the *ion*s and *son*s to obtain the same baseline
323 condition across preparations. However, this often results in a very slow pyloric rhythm,
324 or the pyloric rhythm shutting off entirely (Hamood et al., 2015; Zhang et al., 2009).
325 Therefore, to compare the variability of the pyloric rhythm during Gly^1-SIFamide to a
326 similarly robust pyloric rhythm, we included a comparison of the pyloric rhythm in saline
327 in the intact STNS, in addition to during saline superfusion after *ion*/*son* transection. In
328 an example experiment, the pyloric cycle period was approximately 1.6 s, with a CV of
329 0.02 (Fig. 1Ci, PD activity in the *pdn,* instantaneous cycle period plotted above traces).
330 After *ion*/*son* transection, the pyloric cycle period increased to ~ 2.4 s and a CV of 0.05
331 (Fig.1 Cii). During Gly^1-SIFamide, a gastric mill rhythm was activated, evident in LG and
332 DG neuron bursting (Fig. 1Ciii, *lgn, dgn* recordings) and longer duration gastric mill-
333 timed bursting in the IC neuron (*mvn*). Additionally, the LPG neuron switched from

334 pyloric-only activity (Fig. 1Ci-ii; *lpgn*, Saline conditions) to dual pyloric and gastric mill
335 (slow) bursting (Fig. 1Ciii). Although the average pyloric cycle period in Gly^1-SIFamide
336 (1.6 s) was similar to the intact STNS in this example, there was a visually evident
337 increase in variability (CV = 0.22) (Fig. 1Ciii). The increased variability appeared to be
338 due to three levels of pyloric cycle period (Fig. 1Ciii, colored boxes, discussed in more
339 detail below). When quantified across preparations, we found a consistent increase in
340 pyloric cycle period variability in Gly^1-SIFamide compared to Saline, including both
341 Saline:Intact STNS and after Saline:*ion*/*son* cut (Fig. 1D) (One Way RM ANOVA,
342 $F(18,2) = 30.09$, $p < 0.001$, Table 1). In some experiments there was no active pyloric
343 rhythm to quantify in the Saline:*ions/sons* cut condition and thus points between the
344 Saline:Intact STNS and Gly^1-SIFamide conditions are connected without an
345 intermediate (Saline:*ion*s/*son*s cut) datapoint (see Methods). Thus, compared to the
346 pyloric rhythm when influenced by endogenously active modulatory inputs (Saline:Intact
347 STNS), or a slower pyloric rhythm in the absence of modulatory inputs, the pyloric
348 rhythm cycle period was more variable in the Gly^1-SIFamide modulatory state.

349

350 **Biphasic Regulation of the Pyloric Rhythm**

351 The larger pyloric cycle period CV during Gly^1-SIFamide application appeared to
352 be due to rhythmic changes in cycle period coinciding with activity in some of the gastric
353 mill neurons. Specifically, in example experiments, the pyloric cycle period was longer
354 during times when the IC and LG neurons were active (Figs. 1Ciii, 2A, pink box) relative
355 to pyloric activity when no gastric mill neuron was active (Figs. 1Ciii, 2A; SIFbaseline;
356 grey box; dotted horizontal line across plot of instantaneous cycle period). Shorter

357 duration pyloric cycle periods relative to SIFbaseline coincided with LPG neuron slow
358 bursts (Figs. 1Ciii, 2A; blue box).

359 To further examine the relationship between pyloric cycle period and gastric mill
360 neurons, we measured all pyloric cycle periods across the final 20 min steady-state of
361 30 min Gly^1-SIFamide (5 μM) bath applications and grouped them by the gastric mill
362 neurons that were active. Considering the four gastric mill neurons (LG, LPG, IC, DG),
363 plus the SIFbaseline condition in which no gastric mill neurons are active, there are 16
364 possible combinations of active gastric mill neurons during which a pyloric cycle period
365 might have occurred (Fig. 2B). We focused only on gastric mill-timed bursts (see
366 Methods; Fahoum and Blitz 2024), including for IC and LPG which express dual-
367 network activity. The average cycle period occurring during each neuron or combination
368 of neurons active, per experiment (black dots) and across all experiments (black bars)
369 are plotted for the 16 different combinations (Fig. 2B). Across 19 preparations, there
370 were some preparations in which no pyloric cycle periods overlapped with a
371 combination of neurons. Specifically in the IC, LPG:IC, and LPG:DG:IC categories there
372 were between 9 and 10 preparations with no pyloric cycle periods falling into these
373 categories. In the 13 remaining categories there were 0 to 3 preparations that had no
374 pyloric cycles in these categories. The total number of pyloric cycles that occurred
375 during each condition, across 19 preparations, are indicated above the x axis labels
376 (Fig. 2B; # cycles).

377 We first visually assessed cycle periods as a function of gastric mill neurons
378 active, using a dashed line to highlight the average cycle period across preparations
379 during the SIFbaseline, when no gastric mill neurons were active (grey region, dashed

380 line). Relative to this baseline, the average cycle period per experiment (dots) tended to
381 be shorter in duration than SIFbaseline during LPG activity, whether it was LPG alone
382 or in combination with DG and/or LG neurons (blue region), including the cumulative
383 average cycle period across preparations (black bars) (n = 16-19; Fig. 2B). Conversely,
384 average cycle periods during combinations of IC, DG, and LG activity (pink region)
385 tended to be longer, and thus above SIFbaseline in the graph, including the cumulative
386 average cycle period (IC, n = 9; IC:DG, IC:LG, IC:DG:LG, n = 19). This aligns with an
387 earlier study in which longer pyloric cycle periods correlated with longer duration IC
388 bursts (Blitz et al., 2019). Based on the number of cycles, IC gastric mill-timed bursts
389 most often coincided with LG activity (Fig. 2B, # cycles). Overall, this representation of
390 cycle period as a function of gastric mill neuron activity suggests that LPG, IC, and LG
391 activity may be responsible for the increased variability in pyloric cycle period during the
392 Gly^1-SIFamide gastric mill rhythm compared to saline (Fig. 1D). To analyze this data set
393 statistically, we used a mixed model ANOVA to accommodate the large number of
394 conditions, i.e., combinations of gastric mill neurons active, plus missing values for
395 some combinations (n = 9-19).

396 For the statistical analysis of gastric mill neuron activity on the pyloric cycle
397 period, we considered each gastric mill neuron to be a factor with a full 4-factor within-
398 subjects mixed model ANOVA, including all higher-order interactions. This model
399 indicated statistically significant effects of gastric mill neuron combinations on pyloric
400 cycle period variability ($X^2_{df = 15} = 102.57$, $p < 0.0001$). The model complexity was then
401 iteratively paired down, eliminating non-significant higher-order interactions (Table 2).
402 The most parsimonious model that still explained the variability in pyloric cycle period

403 included single factors LPG, IC, LG and 2-factor terms IC:LPG and IC:LG (Table 2). In
404 this model, there were significant interactions between LG and IC ($X^2_{df = 239}$ = 3.07, p =
405 0.002) and between LPG and IC ($X^2_{df = 238}$ = -2.38, p = 0.02). Specifically, LG had an
406 effect on pyloric cycle period when IC was firing a gastric mill burst (p = 0.0011, Table 2)
407 but not without IC gastric mill activity (p = 0.40, Table 2). However, IC had an effect on
408 cycle period with (p<0.0001) or without LG activity (p=0.48, Table 2), although a weaker
409 effect in the absence of LG. This points to IC playing an important role in the longer
410 cycle pyloric cycle periods, with possible assistance from LG. For the LPG and IC
411 interaction, LPG had an effect on pyloric cycle period with (p < 0.0001) or without (p =
412 0.0004, Table 2) IC generating a gastric mill burst. Similarly, IC affected the pyloric
413 cycle period with (p = 0.008) or without (p < 0.0001, Table 2) LPG firing a gastric mill
414 burst. Thus, from the overlap in timing and the preceding statistical analysis, it appears
415 that IC (possibly LG) and LPG are responsible for the increased and decreased cycle
416 period, respectively, and the consequent higher cycle period variability during the Gly^1-
417 SIFamide gastric mill rhythm. We therefore tested the roles of IC, LG, and LPG in
418 regulating pyloric cycle period by manipulating their activity.
419

420 **IC, but not LG, is responsible for longer pyloric cycle periods**

421 We first addressed whether IC and/or LG were necessary for longer pyloric cycle
422 periods during the Gly^1-SIFamide gastric mill rhythm. The pyloric cycle period was
423 variable in control conditions as is evident in two example experiments (Fig. 3Ai, Bi,
424 *pdn*, instantaneous cycle period plot above traces). This included longer pyloric cycle
425 periods during gastric mill-timed coactivity in LG and IC (Fig. 3; pink boxes). Identified

426 IC gastric mill bursts (see Methods) (Fahoum and Blitz, 2024), are marked with
427 brackets. In one instance in the time range shown, when LG fired a gastric mill burst,
428 but IC produced only pyloric-timed activity that did not reach the level of a gastric mill-
429 timed burst (Fig. 3Ai; grey box), there was no extension of the pyloric cycle period. This
430 is consistent with the statistical analysis of data from figure 2B, that LG had an effect on
431 pyloric cycle period, only when IC was also active (in gastric mill time). To test whether
432 IC and/or LG was responsible for the longer pyloric cycle periods, we reanalyzed a data
433 set from Fahoum and Blitz (2021) in which hyperpolarizing current (-2 to -4 nA) was
434 injected into either IC or LG neurons. In the example experiments, the much longer
435 cycle periods were eliminated when either LG or IC was hyperpolarized (Fig. 3Aii, Bii).
436 When IC was hyperpolarized, LG bursting persisted, and was qualitatively similar to pre-
437 hyperpolarization (Fig. 3Ai-ii). However, when LG was hyperpolarized, IC did not
438 generate any gastric mill-timed bursts, instead its activity was entirely pyloric-timed (Fig.
439 3Bii). Longer pyloric cycle periods, and therefore larger cycle period variability, returned
440 post hyperpolarization, as did IC gastric mill-timed bursting upon removal of
441 hyperpolarizing current into LG (Fig. 3Aiii, Biii).

442 To quantify the results of hyperpolarizing IC and LG, we measured pyloric cycle
443 period CV before (Pre), during (Hype) and after (Post) hyperpolarization (Fig. 4A). The
444 pyloric cycle period CV decreased when IC was hyperpolarized (Fig. 4Ai; black dots and
445 connecting lines indicate results from individual experiments, grey bars indicate
446 averages across experiments) (One Way RM ANOVA, $F(5,2) = 7.43$, $p = 0.01$, Table 3)
447 and when LG was hyperpolarized (Fig. 4Aii; One Way RM ANOVA, $F(3,2) = 6.09$, $p =$
448 0.04, Table 3). We also determined that the pyloric cycle period CV was not altered

449 when DG was hyperpolarized (Fig. 4Aiii; One Way RM ANOVA, $F(3,2) = 1.18$, $p = 0.37$,
450 Table 3) but it was lower when all three gastric mill neurons (IC, LG and DG) were
451 hyperpolarized (Fig. 4Aiv; One Way RM ANOVA, $F(5,2) = 9.13$, $p = 0.01$, Table 3). In
452 the cumulative data, a lower variability when IC or LG or the three gastric mill neurons
453 were hyperpolarized further indicated that IC and/or LG, but not DG, were responsible
454 for regulating pyloric cycle period. When LG was hyperpolarized, IC gastric mill bursting
455 was eliminated in the example experiment in figure 3B. Therefore, we aimed to quantify
456 IC and LG activity across all experiments when either LG or IC was hyperpolarized.
457 However, in 3/4 experiments there were no IC gastric mill bursts when LG was
458 hyperpolarized. Therefore, instead of quantifying IC gastric mill bursts, we reported the
459 number of IC gastric mill bursts before (Pre), during (Hype) and after (Post) LG
460 hyperpolarization (Fig. 4B). There was a reversible decrease in IC gastric mill bursts
461 with LG hyperpolarization (Fig. 4B) (One Way RM ANOVA, $F(3,2) = 22.75$, $p = 0.002$,
462 Table 3). In contrast, when IC was hyperpolarized, LG activity, including burst duration
463 (Fig. 4Ci), firing frequency (Fig. 4Cii) and number of spikes per burst (Fig. 4Ciii) did not
464 change (One Way RM ANOVA; $F(5,2) = 0.04 – 1.52$; all conditions, $p > 0.05$, Table 3).
465 Thus, LG impacts IC activity, but IC does not alter LG activity. It therefore appears likely
466 that hyperpolarizing LG eliminated extended pyloric cycle periods via elimination of IC
467 gastric mill bursting. In combination with a significant contribution of LG to pyloric cycle
468 period variability, only when IC is active (above) these results indicate that IC, but not
469 LG, gastric mill-timed bursts are responsible for the longer pyloric cycle periods.

470

471 **LPG contributes to pyloric cycle period variability in Gly^1-SIFamide**

472 LPG gastric mill-timed activity correlated with decreased pyloric cycle periods
473 (Figs. 1, 2, 5). LPG is electrically coupled to the other pyloric pacemaker neurons (Fig.
474 1B) (Marder and Bucher, 2007; Shruti et al., 2014) and thus hyperpolarizing current
475 injection into the two LPG neurons could alter the pyloric cycle period. Therefore, to test
476 whether LPG was responsible for decreased pyloric cycle periods relative to
477 SIFbaseline (e.g., Fig. 5Ai), the two LPG neurons were photoinactivated (see Methods;
478 LPG:Kill) to selectively remove them from the network, and pyloric cycle periods during
479 Gly^1-SIFamide bath application were compared between LPG:Intact and LPG:Kill.
480 Photoinactivation of two neurons does not alter the response to bath-applied Gly^1-
481 SIFamide, and responses to two consecutive bath applications of Gly^1-SIFamide are not
482 different (Fahoum and Blitz, 2024).

483 In the absence of the LPG neurons (LPG:Kill), the pyloric cycle period variability
484 decreased (Fig. 5Aii) compared to the LPG:Intact condition. Eliminating LPG prevented
485 the periodic decreases in pyloric cycle period. Across experiments, the pyloric cycle
486 period CV was lower after LPG:Kill, compared to LPG:Intact (Fig. 5B; LPG:Intact [blue
487 dots] CV = 0.30 ± 0.03; LPG:Kill [black dots] CV = 0.11 ± 0.03; n = 9; two-tailed paired t-
488 test; $t(8) = 7.78$; $p < 0.001$). However, the decreased variability did not appear to be due
489 to only elimination of shorter pyloric cycle periods. The longer duration pyloric cycle
490 periods were also mostly eliminated in the LPG:Kill condition as can be seen in the
491 example experiment (Fig. 5Aii). Assessing regulation of pyloric cycle period across
492 preparations was complicated by the absence of LPG which eliminated several
493 combinations of active gastric mill neurons. Thus, we chose instead to examine the
494 distribution of cycle periods in the LPG:Intact vs LPG:Kill conditions. There is variability

495 in SIFbaseline pyloric cycle period across preparations (e.g., Fig. 2B, grey box), and
496 photoinactivation of the two LPG neurons shifted the SIFbaseline to shorter pyloric cycle
497 periods (compare instantaneous pyloric cycle period plot in Fig. 5Ai-ii), likely due to
498 removal of “electrical drag” on the pyloric pacemaker neuron AB (Kepler et al., 1990).
499 Thus, to determine whether there was any change in pyloric cycle period regulation
500 between the two conditions, we normalized each pyloric cycle period to the average
501 SIFbaseline cycle period in that preparation and accumulated all normalized pyloric
502 cycle period durations during each condition into their respective histograms (Fig. 5C)
503 (LPG:Intact, blue and LPG:Kill, grey). We also normalized pyloric cycle period count per
504 bin to the highest count for each condition to better enable comparison of the
505 histograms. In the LPG:Intact condition, in addition to the peak around 1 (SIFbaseline,
506 arrowhead), there were shorter pyloric cycle periods (<1; “Shorter” bracket) and a
507 distributed set of bins at longer cycle periods (>1; “Longer” bracket) (Fig. 5C, blue
508 histogram). However, in the LPG:Kill condition (Fig. 5C, grey histogram), there was a
509 single grouping of bars centered around 1 (SIFbaseline) without a population of slower
510 or faster cycle periods. Therefore, removing LPG from the network prevented the
511 increase and the decrease in pyloric cycle period. Electrical coupling between LPG and
512 the pyloric pacemaker can explain why the pyloric rhythm was faster during the strong
513 depolarizations of LPG slow bursts. However, this does not explain why removing LPG
514 also eliminated slowing of the pyloric rhythm. Further, we showed above that IC gastric
515 mill bursting was responsible for extending the pyloric cycle period, slowing the rhythm
516 (Figs. 3-4). This combination of findings led us to ask whether photoinactivation of LPG
517 alters IC gastric mill activity.

518

519 **IC gastric mill bursts were not impacted by LPG photoinactivation**

520 As discussed previously, IC displays both pyloric- and gastric mill-timed bursts,
521 with a gastric mill burst often consisting of multiple pyloric-timed bursts (Fig. 6A). In an
522 example expanded region, a single IC gastric mill burst (Fig. 6Ai, brackets above *mvn*
523 recording) in the LPG:Intact condition consists of four pyloric-timed bursts (Fig. 6Ai,
524 brackets below *mvn* recording). In the LPG:Kill condition, based on established criteria
525 for IC gastric mill bursts (Blitz et al., 2019; Fahoum and Blitz, 2024), a single IC gastric
526 mill burst is approximately the same duration as in the LPG:Intact condition, but consists
527 of seven pyloric bursts, compared to four with LPG neurons intact (Fig. 6A). In a
528 previous study, there was no difference in IC activity between LPG:Intact and LPG:Kill,
529 including no difference in burst duration, firing frequency, and number of spikes per
530 burst for gastric mill bursts and for IC pyloric bursts within IC gastric mill bursts (Fahoum
531 and Blitz, 2024). Because our LPG:Intact, LPG:kill dataset was a subset from the
532 previous study (n = 9/11, see Methods), we reanalyzed the data to verify the result in
533 the specific experiments used here. We found no difference in number of IC gastric mill
534 bursts (Fig. 6Bi; Table 4), IC gastric mill burst duration (s) (Fig. 6Bii; Table 4), number of
535 IC spikes per gastric mill burst (Fig. 6Biii; Table 4), or firing frequency (Hz) (Fig. 6Biv;
536 Table 4). There was also no difference in the number of IC pyloric bursts (Fig. 6Ci;
537 Table 4), IC pyloric burst duration (s) (Fig. 6Cii; Table 4), or IC pyloric firing frequency
538 (Hz) (Fig. 6Civ; Table 4), although there was a trend toward shorter pyloric-timed burst
539 duration (Fig. 6Cii; Table 4), and there was a decrease in the number of spikes per
540 pyloric-timed burst (Fig. 6Ciii; Table 4). The difference between these results and the

541 previous study likely reflects the removal of two preparations in which there was little
542 pyloric regulation in the control condition. For the nine preparations in which there was
543 typical pyloric regulation in control, the tendency for IC pyloric bursts to be shorter, with
544 fewer action potentials in the LPG:Kill condition fits with the loss of long-duration pyloric
545 cycle periods. When longer pyloric cycle periods are eliminated, IC neuron pyloric
546 bursts are shortened as they are interrupted by inhibition from the pyloric pacemaker
547 ensemble at the start of each pyloric cycle (e.g., Fig. 6A). Importantly however, IC
548 gastric mill bursts were not altered by LPG:Kill and IC firing frequency, a measure of the
549 strength of neuronal activity, was not altered for IC gastric mill or pyloric bursts (Fig.
550 6Biv, Civ).

551

552 **Same IC activity level does not slow the pyloric rhythm in the LPG:Kill condition**

553 To determine the relationship between the strength (firing frequency) of IC gastric
554 mill bursts and pyloric cycle period before versus after LPG:Kill, we plotted
555 instantaneous pyloric cycle period against IC firing frequency (Hz) for all pyloric cycles
556 across a 20 min steady state region of Gly^1-SIFamide application for each of nine
557 preparations (Fig. 7). Within a preparation, across the same IC firing frequencies, there
558 were many longer duration pyloric cycle periods in LPG:Intact (blue circles) but many
559 fewer longer duration cycles in the LPG:Kill condition (grey circles) (Fig. 7; n = 9). This
560 indicated that LPG was playing a major role in the ability of IC to increase pyloric cycle
561 period. The occasional ability of IC to increase pyloric cycle period in the absence of
562 LPG indicated a weaker, or only occasionally modulated, connection to the other pyloric
563 pacemaker neurons (PD and AB) (Figs. 7, 8). These data thus suggest that while IC

activity strength is not affected by LPG photoinactivation, its ability to slow the pyloric rhythm requires the presence of LPG.

Discussion

In this study, we show that the cycle period of the faster pyloric rhythm varies between three levels in time with different phases of the related, slower gastric mill rhythm during the Gly^1-SIFamide neuropeptide modulatory state. The LPG neuron switches from pyloric-only activity to dual pyloric and gastric mill activity during Gly^1-SIFamide application (Fahoum and Blitz, 2021; Fahoum and Blitz, 2024; Snyder and Blitz, 2022). Surprisingly, we found that this dual-network LPG neuron is necessary for both phasic increases and phasic decreases in pyloric cycle period during this gastric mill rhythm version. Specifically, the pyloric cycle period decreases during the longer duration, intrinsically-generated gastric mill-timed bursts in LPG, and the pyloric cycle period is prolonged during IC neuron gastric mill bursts which coincide with a silent period in LPG. The complex biphasic regulation of a related network we identify here is distinct in both form and mechanism from previous examples of inter-network coordination in the STNS during other modulatory states, emphasizing the flexible nature of such coordination.

Dual-network Neuron is Necessary for Biphasic Regulation

There are multiple ways in which coordination occurs between different behaviors and between their underlying CPG networks. Here we focused on a single

587 modulatory state and how the activity of one network varies across a single cycle of a
588 second network's activity. Unlike other gastric mill rhythm versions, the Gly^1-SIFamide
589 gastric mill rhythm is triphasic (Blitz et al., 2019; Fahoum and Blitz, 2024). During this
590 triphasic gastric mill rhythm, there is a "baseline" pyloric cycle period due to Gly^1-
591 SIFamide modulatory actions, and the pyloric rhythm is regulated away from this
592 baseline in opposing directions during different phases of the slower gastric mill rhythm.

593 Photoinactivation to selectively eliminate the LPG neurons demonstrated that
594 LPG is necessary for the phasic decreases in pyloric cycle period during the Gly^1-
595 SIFamide gastric mill rhythm. Decreased pyloric cycle periods occur during LPG gastric
596 mill-timed bursts, which are intrinsically generated. In particular, Gly^1-SIFamide
597 enhances excitability and post-inhibitory rebound, and diminishes spike-frequency
598 adaptation in LPG, enabling LPG to generate gastric mill-timed oscillations that do not
599 require any synaptic input (Fahoum and Blitz, 2021; Snyder and Blitz, 2022). An LPG
600 gastric mill-timed burst consists of a sustained depolarization during which LPG intrinsic
601 currents apparently enable it to "escape" the influence of rhythmic hyperpolarizations
602 occurring in its electrically coupled partners, the AB and PD neurons (Blitz et al., 2019;
603 Fahoum and Blitz, 2021; Shruti et al., 2014; Snyder and Blitz, 2022). Electrical
604 synapses are subject to modulation (Kothmann et al., 2009; Lane et al., 2018; O'Brien,
605 2014). Thus, it is possible that Gly^1-SIFamide decreases the strength of electrical
606 coupling between LPG and AB/PD to enable the periodic "escapes". However, the
607 electrical coupling apparently remains functional in Gly^1-SIFamide, as AB/PD pyloric
608 activity is necessary for LPG to generate pyloric bursting in this state (Fahoum and Blitz,
609 2021; Snyder and Blitz, 2022). Further, there is no apparent difference in coupling

610 strength between saline and Gly[1]-SIFamide (Fahoum, Nadim, Blitz, unpublished). In
611 addition to the continued presence of electrical coupling between LPG and AB/PD, we
612 know that 1) decreases in pyloric cycle period require the presence of LPG (this study),
613 2) no other gastric mill neurons are active during LPG gastric mill bursts (Blitz et al.,
614 2019; Fahoum and Blitz, 2024), and 3) LP and IC provide the only known intra-STG
615 feedback to the pyloric pacemakers (Marder and Bucher, 2007; Nadim et al., 2011;
616 Thirumalai et al., 2006; Zhao et al., 2011), but LP is photoinactivated or hyperpolarized
617 and IC is silent or weakly active in pyloric time during this phase (Blitz et al., 2019;
618 Fahoum and Blitz, 2024). Thus, although we are not able to selectively manipulate the
619 electrical synapses between LPG and AB/PD to test our hypothesis, all available
620 evidence indicates that the sustained depolarization during LPG gastric mill bursts has
621 an excitatory effect on the AB/PD neurons to decrease the cycle period of the intrinsic
622 pyloric bursting. This influence occurs despite rectification of the electrical coupling,
623 which favors depolarizing current from AB/PD to LPG, but does allow for some current
624 flow when LPG is depolarized relative to AB/PD (Shruti et al., 2014), which is apparently
625 sufficient to decrease the pyloric cycle period.

626 Unexpectedly, photoinactivation of the LPG neurons also eliminated increases in
627 pyloric cycle period which occur during IC or IC/LG bursting. With LPG intact, we found
628 that LG promotes gastric mill-timed bursting in the IC neuron, but only IC, and not LG, is
629 necessary for the extended pyloric cycle periods. The potential mechanisms for IC-
630 elicited extension of the pyloric cycle period are that gastric mill-timed IC activity directly
631 inhibits some or all of the pyloric pacemaker neurons, or IC gastric mill bursting excites
632 another neuron that inhibits some or all of the pyloric pacemaker neurons. In the Gly[1]-

633 SIFamide gastric mill rhythm, the only neuron besides LG that could be co-active with
634 IC is the LP neuron, which could be “excited” via electrical coupling to IC and does
635 provide inhibitory feedback to the pyloric pacemaker neurons (Nadim et al., 2011;
636 Thirumalai et al., 2006; Weimann and Marder, 1994). However, in our experiments, to
637 mimic the more physiological conditions of Gly^1-SIFamide release from MCN5, with the
638 coincident inhibition of LP via the MCN5 cotransmitter glutamate (Fahoum and Blitz,
639 2021), LP was always photoinactivated or hyperpolarized and therefore could not be
640 inhibiting the pyloric pacemaker neurons. Thus, it is most likely that IC extends pyloric
641 cycle period duration by inhibiting pyloric pacemaker neurons, which include 1 copy of
642 AB, and 2 copies each of PD and LPG.

643 In many modulatory conditions, the AB neuron is a conditional oscillator and the
644 PD and LPG neurons are active in pyloric time due to electrical coupling to AB (Ayali
645 and Harris-Warrick, 1999; Marder and Bucher, 2007). In Gly^1-SIFamide, LPG only
646 generates pyloric-timed bursting if AB/PD do so, but AB/PD do not require LPG to
647 generate pyloric-timed bursting (this study) (Fahoum and Blitz, 2024; Fahoum and Blitz,
648 2021; Snyder and Blitz, 2022). We found that selective photoinactivation of just the two
649 LPG neurons almost entirely eliminated prolonged pyloric cycle periods. One possible
650 explanation for this was that eliminating LPG impacted the activity of IC, however we
651 found no change in IC gastric mill bursts. These results suggest that an IC to LPG
652 synapse is primarily responsible for IC inhibition of the pyloric rhythm, effectively
653 “funneling” IC chemical inhibition through LPG’s electrical coupling to the AB/PD
654 neurons (Fig. 8). In fact, we recently determined that Gly^1-SIFamide enhances a
655 typically ineffective IC to LPG graded glutamatergic synapse, enabling gastric mill IC

656 bursts to regulate LPG gastric mill-timed activity (Fahoum and Blitz, 2023). The current
657 study indicates that the modulated IC to LPG synapse also indirectly regulates the
658 pyloric cycle period via LPG's electrical coupling to AB/PD. Some prolonged pyloric
659 cycle periods in a subset of preparations when LPG was photoinactivated suggests an
660 additional small contribution of an IC to AB and/or PD synapse, however it seems that
661 the main IC regulation of pyloric cycle period occurs via inhibition of LPG (Fig. 8). The
662 reason for IC chemical inhibition to act indirectly via the electrical synapse from LPG to
663 AB/PD is not known. However, it may represent a conservation of function with the IC to
664 LPG synapse playing roles in both gastric mill pattern generation as well as coordination
665 between the pyloric and gastric mill networks.

666 Periodic long-duration IC bursts also inhibit the pyloric rhythm during activation of
667 another modulatory input to the STG, the projection neuron MCN7, which releases the
668 neuropeptide proctolin (Blitz et al., 1999). The specific neuron(s) targeted by IC to
669 extend the pyloric cycle period in the MCN7 rhythm was not determined (Blitz et al.,
670 1999). IC chemical synapses within the STG, including the IC to LPG synapse, are fast
671 inhibitory glutamatergic connections that are blocked by the chloride channel blocker
672 picrotoxin (Fahoum and Blitz, 2024; Marder and Bucher, 2007). Inhibitory neuron
673 connections between networks are implicated in other inter-network interactions,
674 although further exploration is still needed for a mechanistic understanding at the
675 cellular level (Huff et al., 2022).

676

677

678 **Diverse Mechanisms of Inter-network Coordination**

679 Distinct mechanisms have been identified for inter-network coordination in the
680 STNS and other systems. In the STNS, other gastric mill rhythm versions are biphasic,
681 and when pyloric rhythm variability has been quantified, the pyloric period during one
682 phase of the gastric mill rhythm is at a “baseline” period due to modulatory input, and
683 regulated away from this baseline during the other phase of the gastric mill rhythm
684 (Bartos and Nusbaum, 1997). For instance, during a gastric mill rhythm elicited by the
685 modulatory neuron MCN1, the LG neuron presynaptically inhibits MCN1 at its entrance
686 into the STG, rhythmically decreasing modulatory excitation of the pyloric network
687 during the LG phase (Bartos and Nusbaum, 1997; Coleman et al., 1995; Coleman and
688 Nusbaum, 1994; Nusbaum et al., 1992). Thus, there is indirect communication between
689 the two networks via a local feedback synapse. Indirect interactions between networks
690 can also occur via long-distance feedback from network neurons to modulatory inputs or
691 via motor efference copy to related networks (Blitz and Nusbaum, 2008; Lambert et al.,
692 2023; Wood et al., 2004). Although there are both local and long-distance feedback
693 projections to the source of Gly^1-SIFamide (MCN5) (Blitz et al., 2019; Norris et al.,
694 1996), they do not contribute to the inter-network regulation described here, as the
695 neuropeptide was bath-applied. Instead, we found that synapses between network
696 neurons underlie biphasic regulation of the pyloric rhythm.

697 In addition to phasic coordination, there may be correlated changes in the activity
698 levels of related networks such as increased respiratory activity to match more intense
699 forms of locomotion, or increased swallowing occurrences to match increased chewing
700 rates (Hao et al., 2021; Hérent et al., 2023). When the pyloric and gastric mill networks

701 are both active, their activity level is coordinated such that faster pyloric rhythms occur
702 with faster gastric mill rhythms (Bartos et al., 1999; Powell et al., 2021; Saideman et al.,
703 2007). Correlated changes in timing and/or strength can reflect common inputs. In the
704 crab STNS, the modulatory neuron MCN1 acts on both networks, and increasing MCN1
705 firing frequency speeds both rhythms (Bartos et al., 1999; Bartos and Nusbaum, 1997).
706 Similarly, in lamprey, rodents, and cats, the mesencephalic locomotor region provides
707 parallel input to respiratory and locomotor CPGs (Hérent et al., 2023; Juvin et al., 2022;
708 Ryczko and Dubuc, 2013).

709 Some related behaviors display coupling of their activity, with a discrete number
710 of cycles of one pattern occurring relative to a full cycle of the other pattern. Coupling
711 occurs between locomotion and chewing, and locomotion and respiration in humans,
712 other mammals and birds; between whisking and respiration in rodents; and between
713 pyloric and gastric mill rhythms in crustaceans (Bartos et al., 1999; Clemens et al.,
714 1998a; Juvin et al., 2022; Maezawa et al., 2020; Moore et al., 2013; Powell et al., 2021).
715 Coupling of rhythmic behaviors may arise from mechanical forces. For example, flight
716 muscle attachment to structures essential for respiration in birds, and the movement of
717 internal organs in galloping horses may contribute to coupling between locomotion and
718 respiration (Juvin et al., 2022). Similarly, accessory teeth movements are mechanically
719 coupled to the cardiopyloric valve in the stomatogastric system (McGaw and Curtis,
720 2013). However, direct synaptic connections between CPGs can also contribute to this
721 type of inter-network coordination (Juvin et al., 2022). In rodents, proper timing of
722 swallowing within the respiratory cycle, and 1:1 coupling of whisking and fast sniffing,
723 appear to be due to synapses between these related CPGs (Huff et al., 2022; Moore et

724 al., 2013). These coupling ratios between networks are not fixed and can vary during
725 different forms of locomotion, or different breathing behaviors such as fast sniffing and
726 slow breathing (Juvin et al., 2022; Moore et al., 2013; Saunders et al., 2004). In the crab
727 STNS, a direct inhibitory synapse from the pyloric pacemaker neuron AB onto the
728 gastric mill CPG neuron Int1 is essential for coupling between the pyloric and gastric
729 mill rhythms driven by the modulatory neuron MCN1. This inter-network synapse allows
730 the pyloric rhythm to control the speed of the gastric mill rhythm (Bartos et al., 1999;
731 Nadim et al., 1998). However, during the Gly^1-SIFamide rhythm, the speed of the pyloric
732 rhythm does not regulate LPG gastric mill bursting, reinforcing the flexible nature of
733 inter-network coordination (Fahoum and Blitz, 2024).

734 Our results here suggest that the same rectifying electrical synapse alternately
735 reinforces and diminishes modulatory neuropeptide effects on network output. These
736 actions occur due to intrinsic currents enabling reinforcement, and chemical synaptic
737 currents leading to diminished peptide actions. LPG thus serves as a point of
738 convergence for coordination, despite the two network interactions acting in opposite
739 directions. Due to the fluid nature of network composition, dual-network neurons such
740 as LPG provide flexibility by adding and subtracting their activity to different behavioral
741 outputs (Ainsworth et al., 2011; Clapp et al., 2011; Dickinson et al., 1990; Hooper and
742 Moulins, 1989; Roopun et al., 2008; Weimann et al., 1991). Additionally, dual-network
743 neurons can provide flexibility in coordinating network activity by serving as a variable
744 link between networks. This ability however depends on whether they are recruited into
745 new networks as passive followers, or as active components with sufficient synaptic

access to a new network to mediate coordination (Fahoum and Blitz, 2024; Hooper and Moulins, 1990).

Dysfunctional inter-network coordination can impact health and well-being, such as an insufficient oxygen supply relative to metabolic demand if respiration is not coordinated with other motor activity, decreased food intake or choking due to improper coordination of breathing and swallowing, or disrupted communication abilities arising from problems coordinating vocalization and respiration (Barlow, 2009; Juvin et al., 2022; Yagi et al., 2017). Thus, it is important to continue adding to our understanding of inter-network coordination among the many behaviors that require coordination, including understanding how coordination varies across behavioral and environmental conditions (Clemens et al., 1998b; Juvin et al., 2022; Stein and Harzsch, 2021; Stickford and Stickford, 2014).

760 Ainsworth M, Lee S, Cunningham MO, Roopun AK, Traub RD, Kopell NJ, Whittington MA (2011) Dual
761 gamma rhythm generators control interlaminar synchrony in auditory cortex. J Neurosci 31:17040–
762 17051.

763 Anderson T, Garcia AJ, Baertsch NA, Pollak J, Bloom JC, Wei AD, Rai KG, Ramirez JM (2016) A novel
764 excitatory network for the control of breathing. Nature 536:76–80.

765 Ayali A, Harris-Warrick RM (1999) Monoamine control of the pacemaker kernel and cycle frequency in
766 the lobster pyloric network. J Neurosci 19:6712–6722.

767 Barlow SM (2009) Central pattern generation involved in oral and respiratory control for feeding in the
768 term infant. Curr Opin Otolaryngol Head Neck Surg 17:187–193.

769 Barnett WH, Baekey DM, Paton JFR, Dick TE, Wehrwein EA, Molkov YI (2021) Heartbeats entrain
770 breathing via baroreceptor-mediated modulation of expiratory activity. Exp Physiol 106:1181–
771 1195.

772 Bartos M, Manor Y, Nadim F, Marder E, Nusbaum MP (1999) Coordination of fast and slow rhythmic
773 neuronal circuits. J Neurosci 19:6650–6660.

774 Bartos M, Nusbaum MP (1997) Intercircuit control of motor pattern modulation by presynaptic
775 inhibition. J Neurosci 17:2247–2256.

776 Beenhakker MP, Blitz DM, Nusbaum MP (2004) Long-Lasting Activation of Rhythmic Neuronal Activity by
777 a Novel Mechanosensory System in the Crustacean Stomatogastric Nervous System. J Neurosci
778 91:78–91.

779 Blitz DM (2023) Neural circuit regulation by identified modulatory projection neurons. Front Neurosci
780 17.

781 Blitz DM, Christie AE, Coleman MJ, Norris BJ, Marder E, Nusbaum MP (1999) Different proctolin neurons
782 elicit distinct motor patterns from a multifunctional neuronal network. J Neurosci 19:5449–5463.

783 Blitz DM, Christie AE, Cook AP, Dickinson PS, Nusbaum MP (2019) Similarities and differences in circuit
784 responses to applied Gly^1-SIFamide and peptidergic (Gly^1 -SIFamide) neuron stimulation. J
785 Neurophysiol 121:950–972.

786 Blitz DM, Nusbaum MP (2008) State-dependent presynaptic inhibition regulates central pattern
787 generator feedback to descending inputs. J Neurosci 28:9564–9574.

788 Blitz DM, White RS, Saideman SR, Cook A, Christie AE, Nadim F, Nusbaum MP (2008) A newly identified
789 extrinsic input triggers a distinct gastric mill rhythm via activation of modulatory projection
790 neurons. J Exp Biol 211:1000–1011.

791 Bucher D, Haspel G, Golowasch J, Nadim F (2015) Central pattern generators In: ELS , John Wiley & Sons,
792 Ltd: Chichester.

793 Cao Y, Roy S, Sachdev RNS, Heck DH (2012) Dynamic Correlation between Whisking and Breathing
794 Rhythms in Mice. J Neurosci 32:1653–1659.

795 Christie AE, Stein W, Quinlan JE, Beenhakker MP, Marder E, Nusbaum MP (2004) Actions of a
796 histaminergic/peptidergic projection neuron on rhythmic motor patterns in the stomatogastric
797 nervous system of the crab *Cancer borealis*. J Comp Neurol 469:153–169.

798 Clapp WC, Rubens MT, Sabharwal J, Gazzaley A (2011) Deficit in switching between functional brain
799 networks underlies the impact of multitasking on working memory in older adults. Proc Natl Acad
800 Sci U S A 108:7212–7217.

801 Clemens S, Combes D, Meyrand P, Simmers J (1998a) Long-term expression of two interacting motor
802 pattern-generating networks in the stomatogastric system of freely behaving lobster. J
803 Neurophysiol 79:1396–1408.

804 Clemens S, Massabuau JC, Legeay A, Meyrand P, Simmers J (1998b) In vivo modulation of interacting
805 central pattern generators in lobster stomatogastric ganglion: influence of feeding and partial
806 pressure of oxygen. J Neurosci 18:2788–2799.

807 Coleman MJ, Meyrand P, Nusbaum MP (1995) A switch between two modes of synaptic transmission
808 mediated by presynaptic inhibition. Nature 378:502–505.

809 Coleman MJ, Nusbaum MP (1994) Functional consequences of compartmentalization of synaptic input. J
810 Neurosci 14:6544–6552.

811 Daley MA, Bramble DM, Carrier DR (2013) Impact Loading and Locomotor-Respiratory Coordination
812 Significantly Influence Breathing Dynamics in Running Humans. PLoS One 8:70752.

813 Daur N, Nadim F, Bucher D (2016) The complexity of small circuits: the stomatogastric nervous system.
814 Curr Opin Neurobiol 41:1–7.

815 Demartsev V, Manser MB, Tattersall GJ (2022) Vocalization-associated respiration patterns:
816 thermography-based monitoring and detection of preparation for calling. J Exp Biol 225.

817 Dickinson PS, Mecsas C, Marder E (1990) Neuropeptide fusion of two motor-pattern generator circuits.
818 Nature 344:155–157.

819 Dickinson PS, Stemmler EA, Cashman CR, Brennan HR, Dennison B, Huber KE, Peguero B, Rabacal W,
820 Goiney CC, Smith CM, Towle DW, Christie AE (2008) SIFamide peptides in clawed lobsters and
821 freshwater crayfish (Crustacea, Decapoda, Astacidea): A combined molecular, mass spectrometric
822 and electrophysiological investigation. Gen and Comp Endocrinol 156:347–360.

823 Fahoum S-RH, Blitz DM (2023) Neuropeptide Modulation of Bidirectional Internetwork Synapses. bioRxiv
824 2023.12.15.571956.

825 Fahoum S-RH, Blitz DM (2024) Switching neuron contributions to second network activity. J
826 Neurophysiol 131:417–434.

827 Fahoum S-RH, Blitz DM (2021) Neuronal switching between single- and dual-network activity via
828 modulation of intrinsic membrane properties. J Neurosci 41:7848–7863.

829 Fortune ES, Rodríguez C, Li D, Ball GF, Coleman MJ (2011) Neural mechanisms for the coordination of
830 duet singing in wrens. Science 334:666–670.

831 Gariépy JF, Missaghi K, Dubuc R (2010) The interactions between locomotion and respiration. Prog Brain
832 Res 187:173–188.

833 Grillner S, El Manira A (2020) Current principles of motor control, with special reference to vertebrate
834 locomotion. Physiol Rev 100:271–320.

835 Gutierrez GJ, Grashow RG (2009) *Cancer borealis* stomatogastric nervous system dissection. J Vis Exp
836 23:1–5.

837 Hamood AW, Haddad SA, Otopalik AG, Rosenbaum P, Marder E (2015) Quantitative reevaluation of the
838 effects of short- and long-term removal of descending modulatory inputs on the pyloric rhythm of
839 the crab, *Cancer borealis*. eNeuro 2:1–13.

840 Hao N, Sasa A, Kulvanich S, Nakajima Y, Nagoya K, Magara J, Tsujimura T, Inoue M (2021) Coordination
841 of Respiration, Swallowing, and Chewing in Healthy Young Adults. Front Physiol 12:696071.

842 Hérent C, Diem S, Usseglio G, Fortin G, Bouvier J (2023) Upregulation of breathing rate during running
843 exercise by central locomotor circuits in mice. Nat Commun 14:2–17.

844 Higashino M, Miyata K, Kudo K (2022) Coordination dynamics of thoracic and abdominal movements
845 during voluntary breathing. Sci Rep 12:13266.

846 Hooper SL, Moulins M (1990) Cellular and synaptic mechanisms responsible for a long-lasting
847 restructuring of the lobster pyloric network. J Neurophysiol 64:1574.

848 Hooper SL, Moulins M (1989) Switching of a neuron from one network to another by sensory-induced
849 changes in membrane properties. Science 244:1587–1589.

850 Hooper SL, Thuma JB, Guschlbauer C, Schmidt J, Büschges A (2015) Cell dialysis by sharp electrodes can
851 cause nonphysiological changes in neuron properties. J Neurophysiol 114:1255–1271.

852 Huff A, Karlen-Amarante M, Pitts T, Marino Ramirez J (2022) Optogenetic stimulation of pre-Botzinger
853 complex reveals novel circuit interactions in swallowing-breathing coordination. PNAS 119:1–11.

854 Huybrechts J, Nusbaum MP, Bosch L Vanden, Baggerman G, De Loof A, Schoofs L (2003)
855 Neuropeptidomic analysis of the brain and thoracic ganglion from the Jonah crab, *Cancer borealis*.
856 Biochem Biophys Res Commun 308:535–544.

857 Juvin L, Colnot E, Barrière G, Thoby-Brisson M, Morin D (2022) Neurogenic mechanisms for locomotor-
858 respiratory coordination in mammals. Front Neuroanat 16.

859 Kepler TB, Marder EVE, Abbott LF (1990) The effect of electrical coupling on the frequency of model
860 neuronal oscillators. Science 248:83–85.

861 Kothmann WW, Massey SC, O'Brien J (2009) Dopamine-stimulated dephosphorylation of connexin 36
862 mediates AII amacrine cell uncoupling. J Neurosci 29:14903–14911.

863 Lambert FM, Beraneck M, Straka H, Simmers J (2023) Locomotor efference copy signaling and gaze
864 control: An evolutionary perspective. Curr Opin Neurobiol 82.

865 Lane BJ, Kick DR, Wilson DK, Nair SS, Schulz DJ (2018) Dopamine maintains network synchrony via direct
866 modulation of gap junctions in the crustacean cardiac ganglion. Elife 7:e39368.

867 Maezawa H, Koganemaru S, Matsuhashi M, Hirata M, Funahashi M, Mima T (2020) Entrainment of
868 chewing rhythm by gait speed during treadmill walking in humans. Neurosci Res 156:88–94.

869 Marder E, Bucher D (2007) Understanding circuit dynamics using the stomatogastric nervous system of
870 lobsters and crabs. Ann Rev Physiol 69:291–316.

871 McGaw IJ, Curtis DL (2013) A review of gastric processing in decapod crustaceans. J Comp Physiol B
872 183:443–465.

873 Moore JD, Deschênes M, Furuta T, Huber D, Smear MC, Demers M, Kleinfeld D (2013) Hierarchy of
874 orofacial rhythms revealed through whisking and breathing. Nature 2013 497:7448 497:205–210.

875 Mulloney B, Smarandache-Wellmann C (2012) Neurobiology of the crustacean swimmeret system. Prog
876 Neurobiol 96:242–267.

877 Nadim F, Manor Y, Nusbaum MP, Marder E (1998) Frequency regulation of a slow rhythm by a fast
878 periodic input. J Neurosci 18:5053–5067.

879 Nadim F, Zhao S, Zhou L, Bose A (2011) Inhibitory feedback promotes stability in an oscillatory network.
880 J Neural Eng 8.

881 Norris BJ, Coleman MJ, Nusbaum MP (1996) Pyloric motor pattern modification by a newly identified
882 projection neuron in the crab stomatogastric nervous system. J Neurophysiol 75:97–108.

883 Nusbaum MP, Beenhakker MP (2002) A small-systems approach to motor pattern generation. Nature
884 417:343–350.

885 Nusbaum MP, Weimann JM, Golowasch J, Marder E (1992) Presynaptic control of modulatory fibers by
886 their neural network targets. J Neurosci 12:2706–2714.

887 O'Brien J (2014) The ever-changing electrical synapse. Curr Opin Neurobiol 29:64–72.

888 Okobi DE, Banerjee A, Matheson AMM, Phelps SM, Long MA (2019) Motor cortical control of vocal
889 interaction in neotropical singing mice. Science 363:983–988.

890 Powell D, Haddad SA, Gorur-Shandilya S, Marder E (2021) Coupling between fast and slow oscillator
891 circuits in *Cancer borealis* is temperature-compensated. Elife 10:e60454.

892 Ramirez J-M, Baertsch N (2018) Defining the rhythmogenic elements of mammalian breathing.
893 Physiology 33:302–316.

894 Roopun AK, Kramer MA, Carracedo LM, Kaiser M, Davies CH, Traub RD, Kopell NJ, Whittington MA
895 (2008) Temporal interactions between cortical rhythms. Front Neurosci 2:145–154.

896 Ryczko D, Dubuc R (2013) The multifunctional mesencephalic locomotor region. Curr Pharm Des
897 19:4448–4470.

898 Saideman SR, Blitz DM, Nusbaum MP (2007) Convergent motor patterns from divergent circuits. J
899 Neurosci 27:6664–6674.

900 Saunders SW, Rath D, Hodges PW (2004) Postural and respiratory activation of the trunk muscles
901 changes with mode and speed of locomotion. Gait Posture 20:280–290.

902 Shruti S, Schulz DJ, Lett KM, Marder E (2014) Electrical coupling and innexin expression in the
903 stomatogastric ganglion of the crab *Cancer borealis*. J Neurophysiol 112:2946–2958.

904 Sillar KT, Simmers J, Combes D (2023) From tadpole to adult frog locomotion. Curr Opin Neurobiol
905 82:102753.

906 Snyder RR, Blitz DM (2022) Multiple intrinsic membrane properties are modulated in a switch from
907 single- to dual-network activity. J Neurophysiol 128:1181–1198.

908 Spencer RM, Blitz DM (2016) Network feedback regulates motor output across a range of modulatory
909 neuron activity. J Neurophysiol 115:3249–3263.

910 Stein W, Harzsch S (2021) The neurobiology of ocean change – insights from decapod crustaceans.
911 Zoology 144:125887.

912 Stickford ASL, Stickford JL (2014) Ventilation and locomotion in humans: Mechanisms, implications, and
913 perturbations to the coupling of these two rhythms. Springer Sci Rev 2:95–118.

914 Thirumalai V, Prinz AA, Johnson CD, Marder E (2006) Red pigment concentrating hormone strongly
915 enhances the strength of the feedback to the pyloric rhythm oscillator but has little effect on
916 pyloric rhythm period. J Neurophysiol 95:1762–1770.

917 Wei XP, Collie M, Dempsey B, Fortin G, Yackle K (2022) A novel reticular node in the brainstem
918 synchronizes neonatal mouse crying with breathing. Neuron 110:644-657.e6.

919 Weimann JM, Marder E (1994) Switching neurons are integral members of multiple oscillatory networks.
920 Current Biology 4:896–902.

921 Weimann JM, Meyrand P, Marder E (1991) Neurons that form multiple pattern generators:
922 Identification and multiple activity patterns of gastric/pyloric neurons in the crab stomatogastric
923 system. J Neurophysiol 65:111–122.

924 Wood DE, Manor Y, Nadim F, Nusbaum MP (2004) Intercircuit control via rhythmic regulation of
925 projection neuron activity. J Neurosci 24:7455–7463.

926 Yagi N, Oku Y, Nagami S, Yamagata Y, Kayashita J, Ishikawa A, Domen K, Takahashi R (2017)
927 Inappropriate Timing of Swallow in the Respiratory Cycle Causes Breathing-Swallowing
928 Discoordination. Front Physiol 8:676.

929 Yasuda A, Yasuda-Kamatani Y, Nozaki M, Nakajima T (2004) Identification of GYRKPPFNGSIFamide
930 (crustacean-SIFamide) in the crayfish *Procambarus clarkii* by topological mass spectrometry
931 analysis. Gen and Comp Endocrinol 135:391–400.

932 Zhang Y, Khorkova O, Rodriguez R, Golowaschi J (2009) Activity and neuromodulatory input contribute
933 to the recovery of rhythmic output after decentralization in a central pattern generator. J
934 Neurophysiol 101:372–386.

935 Zhao S, Sheibanie AF, Oh M, Rabbah P, Nadim F (2011) Peptide neuromodulation of synaptic dynamics in
936 an oscillatory network. J Neurosci 31:13991–14004.

937

938

939 **Figure Legends**

940 **Figure 1. Gly^1-SIFamide elicited a variable pyloric rhythm**. ***A*,** Schematic of the
941 isolated stomatogastric nervous system (STNS) of the crab, *Cancer borealis*. The STNS
942 consists of the paired commissural ganglia (CoG), the single oesophageal ganglion
943 (OG) and the single stomatogastric ganglion (STG), plus motor and connecting nerves.
944 The STG consists of neuropil and the cell bodies of both the gastric mill and pyloric
945 network neurons. The line breaks on the *ion* and *son* indicate where they were cut to
946 isolate the STG network (Saline:*ions/sons* cut). Two compartments were created with a
947 Vaseline wall across the dish and separately superfused. Gly^1-SIFamide (5 μM) was
948 bath-applied selectively to the posterior compartment containing the STG. ***B*,** Schematic
949 of the pyloric and gastric mill connectome. Resistor symbols indicate electrical coupling,
950 diode symbols indicate rectification of electrical coupling, and ball and stick symbols
951 indicate chemical inhibition. Colors indicate neurons that participate in the Gly^1-
952 SIFamide rhythm and are discussed in this study. ***C*,** Representative
953 electrophysiological traces of the pyloric (*pdn*, *mvn, lpgn*) and gastric mill (*mvn, dgn* and
954 *lgn*) networks in an example experiment in Saline:Intact STNS (**Ci**), Saline:*ions/sons* cut
955 (**Cii**) and bath-applied Gly^1-SIFamide (5 μM) (**Ciii**) conditions. The instantaneous pyloric
956 cycle period is plotted at the top of each set of traces. All conditions are from the same
957 experiment. The colored boxes indicate three levels of pyloric cycle period, overlapping
958 with three distinct phases of the Gly^1-SIFamide gastric mill rhythm (blue: LPG activity;
959 pink: IC/LG activity; grey: baseline Gly^1-SIFamide modulation when no gastric mill
960 neurons are active; see also Fig. 2). ***D*,** The coefficient of variation (CV) of the pyloric
961 cycle period is plotted for three experimental conditions: 1) in saline prior to isolation of

962 the STG network (Saline:Intact STNS, n = 19), 2) in saline with *ions/son*s cut to isolate
963 the STG network from descending modulatory inputs (Saline:*ion*s/*son*s cut, n = 12) and
964 3) during 5 μM Gly^1-SIFamide bath application (SIFamide, n = 19). Each dot represents
965 individual experiments and lines connecting across the experimental conditions depict
966 data points from the same preparation. The different n-value for *ion*s/*son*s cut is due to
967 the lack of a pyloric rhythm in seven preparations in this condition. In the absence of
968 modulatory inputs, the pyloric rhythm sometimes shuts off (Zhang et al., 2009; Hamood
969 et al., 2015). ***$p < 0.001$, One Way RM ANOVA, Holm-sidak *post hoc*. Neurons: AB,
970 anterior burster; AM, anterior median; DG, dorsal gastric; GM, gastric mill; IC, inferior
971 cardiac; Int1, Interneuron 1; LG, lateral gastric; LP, lateral pyloric; LPG, lateral posterior
972 gastric; MG, medial gastric; PD, pyloric dilator; PY, pyloric; VD, ventricular dilator.
973 Nerves: *dgn*, dorsal gastric nerve; *ion*, inferior oesophageal nerve; *lgn*, lateral gastric
974 nerve; *lpgn*, lateral posterior gastric nerve; *lvn*, lateral ventricular nerve; *mvn*, median
975 ventricular nerve; *pdn*, pyloric dilator nerve; *son*, superior oesophageal nerve; *stn*,
976 stomatogastric nerve.

977

978 **Figure 2. Pyloric cycle periods occurred at three different levels during the Gly^1-**
979 **SIFamide gastric mill rhythm**. ***A*,** The pyloric rhythm occurs with a shorter cycle period
980 during LPG activity (blue box), with a longer cycle period during LG:IC activity (pink box)
981 and an intermediate level in the absence of any gastric mill-timed bursting (SIFbaseline;
982 grey box). Representative traces show an example rhythm during Gly^1-SIFamide bath
983 application, with instantaneous pyloric cycle period plotted at the top. Dotted line across
984 instantaneous cycle period plot indicates SIFbaseline cycle period. ***B*,** The average

985 pyloric cycle period is plotted for no gastric mill neuron activity (SIFbaseline; grey box)
986 and during activity of each combination of 1, 2, 3, and 4 gastric mill neurons (n = 19).
987 Each dot represents the average pyloric cycle period during that particular neuron
988 activity across a 20 min analysis window during Gly^1-SIFamide steady state in a single
989 experiment. Black bars indicate the mean pyloric cycle period across all experiments
990 during that neuronal activity. Numbers at the bottom of the graph depict the total
991 number of pyloric cycles contributing to the averages for that neuronal activity. Dotted
992 line represents average pyloric cycle period during SIFbaseline (grey box). Blue box
993 highlights neuronal activity combinations that include LPG, and pink box highlights
994 combinations that include IC.

995

996 **Figure 3. IC or LG hyperpolarization eliminated longer cycle periods and**
997 **decreased pyloric cycle period variability.** ***A***, Extracellular and intracellular
998 recordings monitor the pyloric rhythm (*pdn*) and gastric mill-timed bursting in the IC and
999 LG neurons in control (Pre; ***Ai***, ***Bi***; Top), during IC (***Aii***) or LG (***Bii***) hyperpolarization,
1000 and after hyperpolarization (Post; ***Aiii***, ***Biii***), all during Gly^1-SIFamide bath application. A
1001 and B are from different experiments. Pyloric cycle period on top of the extracellular *pdn*
1002 recording plots the instantaneous pyloric cycle period during each condition. Note the
1003 absence of longer pyloric cycle periods during both LG and IC hyperpolarization (pink
1004 boxes indicate LG:IC activity, grey box indicates LG activity without an IC gastric mill
1005 burst (Ai). IC gastric mill bursts are identified by brackets above the IC recordings.
1006 Downward filled arrowheads indicate hyperpolarizing current injection (Aii and Bii).

1007 Downward white arrowheads above instantaneous pyloric cycle period indicate the
1008 SIFbaseline cycle period (dashed line).

1009

1010 **Figure 4. IC hyperpolarization decreased pyloric cycle period variability without**
1011 **altering LG activity.** ***A***, The average CV of pyloric cycle period across 200 sec
1012 windows is plotted for IC (***Ai***, n = 6), LG (***Aii***, n = 4), DG (***Aiii***, n = 4) or all three neurons
1013 (***Aiv***, n = 6) before (Pre), during (Hype) and after (Post) hyperpolarization. ***B***, The
1014 number of IC gastric mill bursts (burst duration > 0.45 s) occurring before (Pre), during
1015 (Hype) and after (Post) LG hyperpolarization is plotted (n = 4). ***C***, LG burst duration (***Ci***),
1016 firing frequency (***Cii***) and number of spikes per burst (***Civ***) before (Pre), during (Hype)
1017 and after (Post) IC hyperpolarization are plotted (n = 6). For all graphs, data points
1018 represent individual experiments connected by lines across conditions. Grey bars
1019 indicate the average across experiments. *$p < 0.05$, One Way RM ANOVA, Holm-sidak
1020 *post hoc* test.

1021

1022 **Figure 5. LPG photoinactivation decreased pyloric cycle period variability in Gly^1-**
1023 **SIFamide**. ***Ai,*** In control Gly^1-SIFamide with LPG neurons intact, there are shorter cycle
1024 periods during LPG gastric mill-timed bursts (blue box), compared to SIFbaseline
1025 (dashed line) and longer cycle periods during IC activity (pink box). ***Aii***, After both LPG
1026 neurons were photoinactivated (see Methods), pyloric cycle period variability appeared
1027 lower. Pink box highlights an IC gastric mill burst (group of pyloric-timed bursts > 0.45 s
1028 duration). The small units in the *lpgn* recording are PY neurons. ***B***, The pyloric cycle

1029 period coefficient of variation (CV) is plotted for a 20 min window of steady state activity
1030 in the LPG:Intact (blue dots) and LPG:Kill (black dots) conditions (n = 9). Each pair of
1031 dots plus their connecting lines represents a single preparation. Grey bars indicate the
1032 average CV across experiments in each condition. ***$p < 0.001$, paired t-test. ***C***,
1033 Overlaid histograms (bin size: 3 ms) of all pyloric cycle periods across 20 min windows
1034 during steady state Gly^1-SIFamide application in the LPG:Intact (blue) and LPG:Kill
1035 (grey) conditions (n = 9). Each individual cycle period was normalized to the average
1036 SIFbaseline of the same preparation. Bin count of each condition was normalized to the
1037 peak count of that condition to facilitate comparison of histograms. Brackets on top of
1038 histogram indicate shorter pyloric cycle periods, SIFbaseline (arrow) and longer pyloric
1039 cycle periods.

1040

1041 **Figure 6. IC firing frequency was not affected by LPG photoinactivation. *A***,
1042 Representative traces illustrate differences in IC gastric mill-timed activity (brackets on
1043 top of *mvn* recording) before (***Ai***, LPG:Intact) and after (***Aii***, LPG:Kill) photoinactivation
1044 of the two LPG neurons. Pyloric-timed IC bursts within each IC gastric mill burst were
1045 identified if there was a gap between IC action potentials that coincided with a PD
1046 neuron burst (brackets below *mvn* recording). ***B***, IC gastric mill-timed activity was
1047 quantified across 20 min windows during steady state Gly^1-SIFamide bath application,
1048 including number of bursts (***Bi***), burst duration (***Bii***), number of spikes/burst (***Biii***), and
1049 firing frequency (***Biv***). ***C***, IC pyloric-timed activity within each gastric mill-timed burst
1050 was also quantified, including number of bursts (***Ci***) burst duration (***Cii***), number of
1051 spikes/burst (***Ciii***), and firing frequency (***Civ***). Blue dots indicate LPG:Intact condition

1052 and black dots indicate LPG:Kill condition. All dots represent the average within an
1053 experiment with lines connecting the two conditions in each experiment. Grey bars
1054 indicate averages across experiments. *$p < 0.05$, paired t-test.

1055

1056 **Figure 7. The same IC firing frequency did not alter pyloric cycle period in the**
1057 **absence of LPG neurons.** Instantaneous pyloric cycle period is plotted against IC firing
1058 frequency in the LPG:Intact (blue dots) and LPG:Kill (grey dots) during 20 min windows.
1059 Each graph plots the data from a single experiment and each dot represents the
1060 instantaneous pyloric cycle period and the IC firing frequency within its pyloric-timed
1061 burst during the same pyloric cycle. Only cycle periods overlapping with IC gastric mill
1062 bursts (IC bursts > 0.45 s; see Fig. 6) are plotted.

1063

1064 **Figure 8. During the Gly^1-SIFamide modulatory state, gastric mill bursting in LPG**
1065 **decreases pyloric cycle period, while gastric mill bursting in the IC neuron**
1066 **requires LPG to prolong the pyloric cycle period.**

1067 In saline (*Left*, black traces and circuitry), LPG is active only in pyloric time, coincident
1068 with the AB/PD pyloric pacemaker neurons. Gly^1-SIFamide (*Right*, green bar), elicits a
1069 unique gastric mill rhythm (Blitz et al., 2019; Fahoum and Blitz 2021, 2024), during
1070 which the pyloric cycle period varies between a baseline level due to Gly^1-SIFamide
1071 modulation (grey), shorter periods which occur during LPG gastric mill-timed slow
1072 bursting (blue) and longer periods which occur during IC gastric mill bursting (pink).
1073 Gastric mill bursting in LPG (blue box, G: gastric mill burst) likely allows sufficient

1074 current though the rectifying electrical synapses (diode symbol) to the AB and PD
1075 neurons to decrease the cycle period of the pyloric rhythm (blue). IC gastric mill bursting
1076 (pink burst; G: gastric mill burst) is necessary for rhythmic increases in cycle period of
1077 the pyloric rhythm (pink). However, this inhibition appears to act primarily via IC
1078 chemical synaptic inhibition of LPG (thick pink stick/ball), with a possible weak
1079 contribution via chemical inhibition of the AB and/or PD neuron (thin pink line/ball). The
1080 IC to LPG inhibitory synapse is strengthened during Gly^1-SIFamide modulation
1081 (compare thin line/ball in saline to thick line/ball in Gly^1-SIFamide; Fahoum and Blitz,
1082 2023).

1083

1084 Table 1. Pyloric cycle period CV in saline (intact STNS or with *ion*s/*son*s transected) and during
1085 bath application of Gly[1]-SIFamide (5 μM).

Pyloric Cycle Period CV Mean ± SEM				p-value		
Saline:Intact STNS (n = 19)	Saline:*ion*/*son* cut (n = 12)	Gly[1]-SIFamide (n = 19)	F (df)	Saline:Intact STNS vs SIFamide	Saline:*ion*/*son* cut vs SIFamide	Saline:Intact STNS vs Saline:*ion*/*son* cut
0.03 ± 0.002	0.08 ± 0.01	0.29 ± 0.04	30.09 (18,2)	<0.001	<0.001	0.182

1086 One-way repeated measures ANOVA, Holm-Sidak *post hoc*; CV, coefficient of variation; df,
1087 degrees of freedom

1088

Table 2. Statistical analysis of active gastric mill neuron contributions to pyloric cycle period variability during Gly[1]-SIFamide (5 μM) application.

Model Complexity		$X^{2(a,b)}$, df t^{c}, df	p-value
4-factor interaction term removed		0.0612[a], 1	0.8047
All 3-factor interaction terms removed		2.9444[b], 4	0.5672
Final Model:		1.019[b], 5	0.961
Includes LPG, LG, IC, LPG:IC, LG:IC		4.015[a], 10	0.946
Post hoc comparisons of significant 2-factor interactions in final model	LG with IC Present	-3.30[c], 240	0.011
	LG with IC Absent	0.84[c], 239	0.40
	IC with LG Present	-7.15[c], 238	<0.0001
	IC with LG Absent	-1.99[c], 241	0.048
	LPG with IC Present	-6.35[c], 238	<0.0001
	LPG with IC Absent	-3.57[c], 238	0.0004
	IC with LPG Present	-2.69[c], 239	0.008
	LPG with IC Absent	-6.23[c], 238	<0.0001

4-factor within-subjects mixed model ANOVA with iterative elimination of non-significant higher-order interactions. Models were compared to full model[a] or previous level of complexity[b] using a likelihood ratio test. [C]*post hoc* comparisons of estimated marginal means.

1111 Table 3. Pyloric cycle period CV and IC and LG gastric mill activity in Gly[1]-SIFamide (5 μM)
1112 before, during, and after hyperpolarization of gastric mill neurons.

Manipulation	Parameter	Mean ± SEM			F (df)	p-value		
		Pre	Hype	Post		Pre vs Hype	Hype vs Post	Pre vs Post
Hype IC (n = 6)	Pyloric Cycle Period CV	0.30± 0.06	0.09± 0.02	0.25± 0.07	7.43 (5,2)	0.01	0.04	0.39
Hype LG (n = 4)		0.28± 0.09	0.06± 0.02	0.17±4 0.06	6.09 (3,2)	0.04	0.15	0.22
Hype DG (n = 4)		0.21± 0.05	0.19± 0.06	0.17± 0.04	1.18 (3,2)	ns	ns	ns
Hype IC/LG/DG (n = 6)		0.27± 0.066	0.10± 0.05	0.26± 0.06	9.13 (5,2)	0.01	0.01	0.86
Hype LG (n = 4)	# IC Bursts	12.75± 1.80	1.50± 1.50	12.75± 1.44	22.75 (3,2)	0.003	0.002	1
Hype IC (n = 6)	LG Burst Duration (s)	4.63± 1.01	5.08± 0.95	6.51± 1.25	1.52 (5,2)	ns	ns	ns
	LG # Spikes/Burst	15.34± 5.16	16.50± 5.54	21.79± 5.73	0.49 (5,2)	ns	ns	ns
	LG Firing Freq. (Hz)	2.90± 0.39	2.91± 0.49	3.07± 0.46	0.04 (5,2)	ns	ns	ns

1113 Pre, before hyperpolarization of neuron(s); Hype, during hyperpolarization of neuron(s); Post,
1114 after hyperpolarization of neuron(s); CV, coefficient of variation; df, degrees of freedom; ns, p*ost*
1115 *hoc* not performed when $p > 0.05$; One-way repeated measures ANOVA, Holm-Sidak *post hoc*

1116

1117 Table 4. IC gastric mill- and pyloric-timed activity during LPG Intact and LPG

1118 photoinactivated (Killed) conditions in Gly[1]-SIFamide (5 μM).

		Mean ± SEM			
		LPG Intact	LPG Killed	*t, df*	*p-value*
IC Gastric mill bursts (n = 9)	# bursts	68.89 ± 9.50	68.33 ± 9.98	0.12, 8	0.91
	Burst Duration (s)	5.08 ± 0.65	4.33 ± 0.34	1.48, 8	0.18
	# Spikes/Burst	64.59 ± 9.53	55.02 ± 7.04	1.71, 8	0.13
	Firing Freq. (Hz)	12.96 ± 1.02	12.47 ± 0.86	0.93, 8	0.37
IC, pyloric bursts (n = 9)	# bursts	249.56 ± 35.09	262.22 ± 35.02	-0.78, 8	0.46
	Burst Duration (s)	1.31 ± 0.14	1.01 ± 0.20	2.00, 8	0.08
	# Spikes/Burst	19.02 ± 2.16	13.37 ± 2.03	2.81, 8	0.02
	Firing Freq. (Hz)	14.14 ± 1.61	13.83 ± 1.72	0.65, 8	0.53

1119 During Gly[1]-SIFamide application; paired t-test

1120

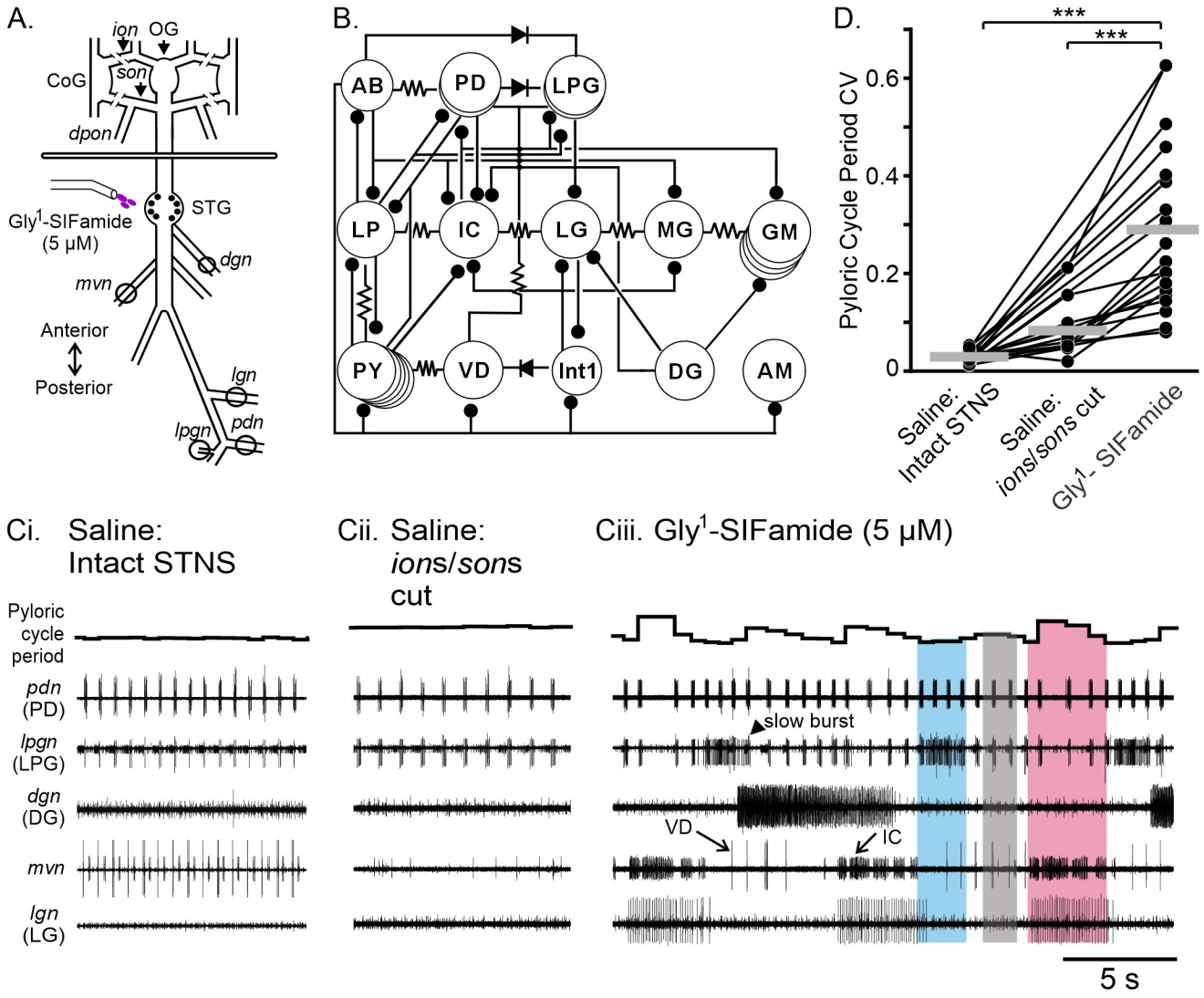

Figure 1
Gnanabharathi, Fahoum & Blitz

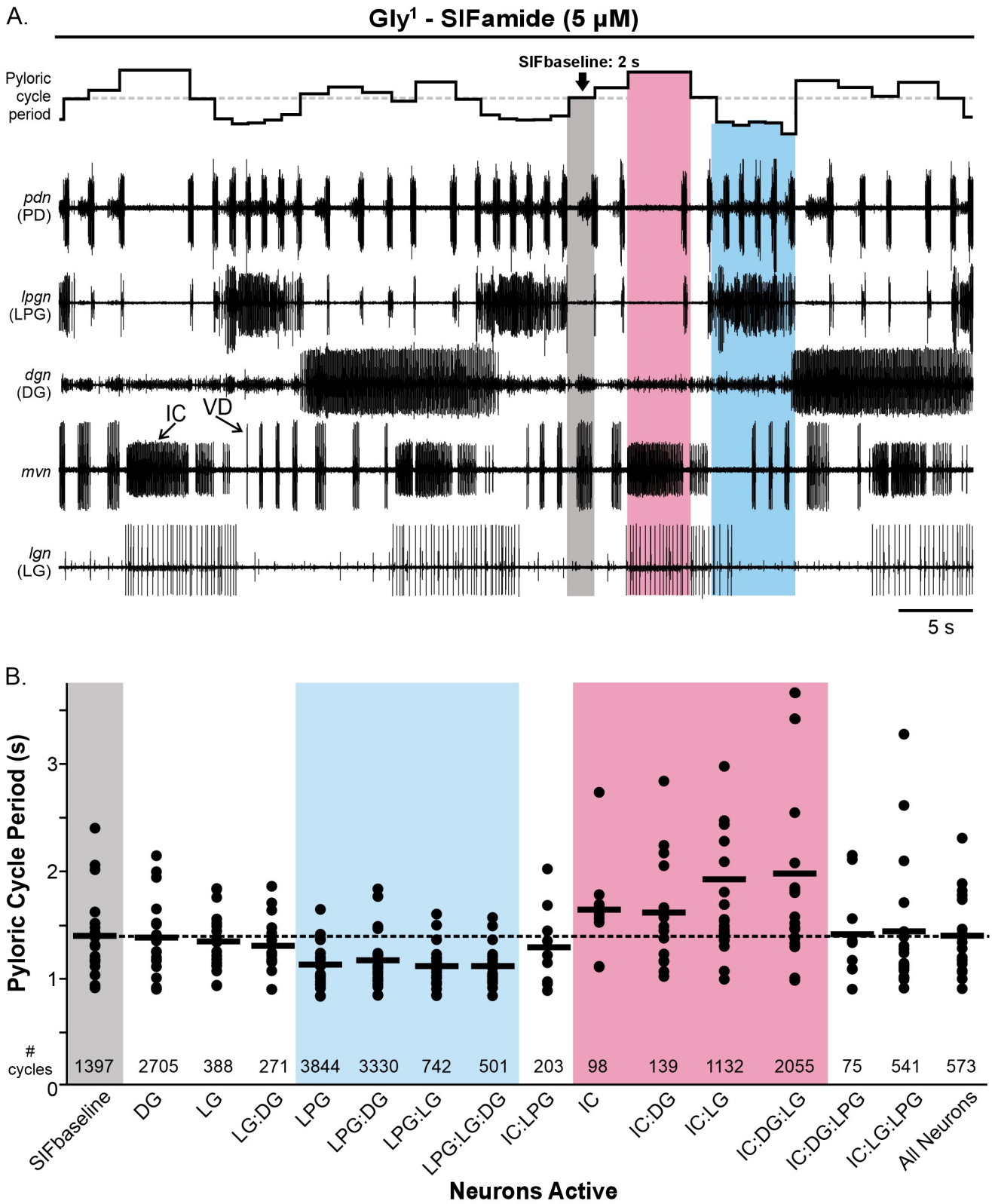

Figure 2
Gnanabharathi, Fahoum & Blitz

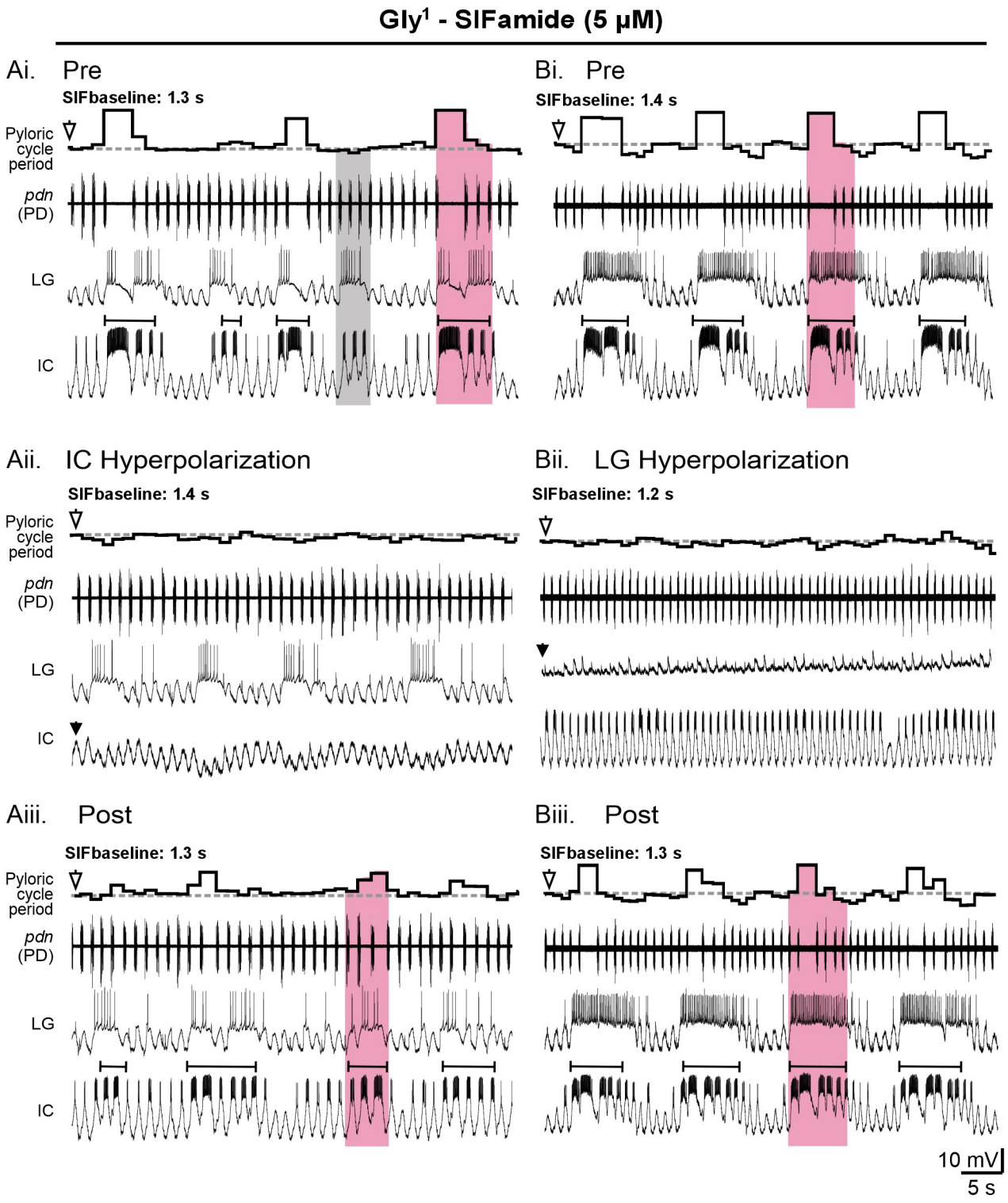

Figure 3
Gnanabharathi, Fahoum & Blitz

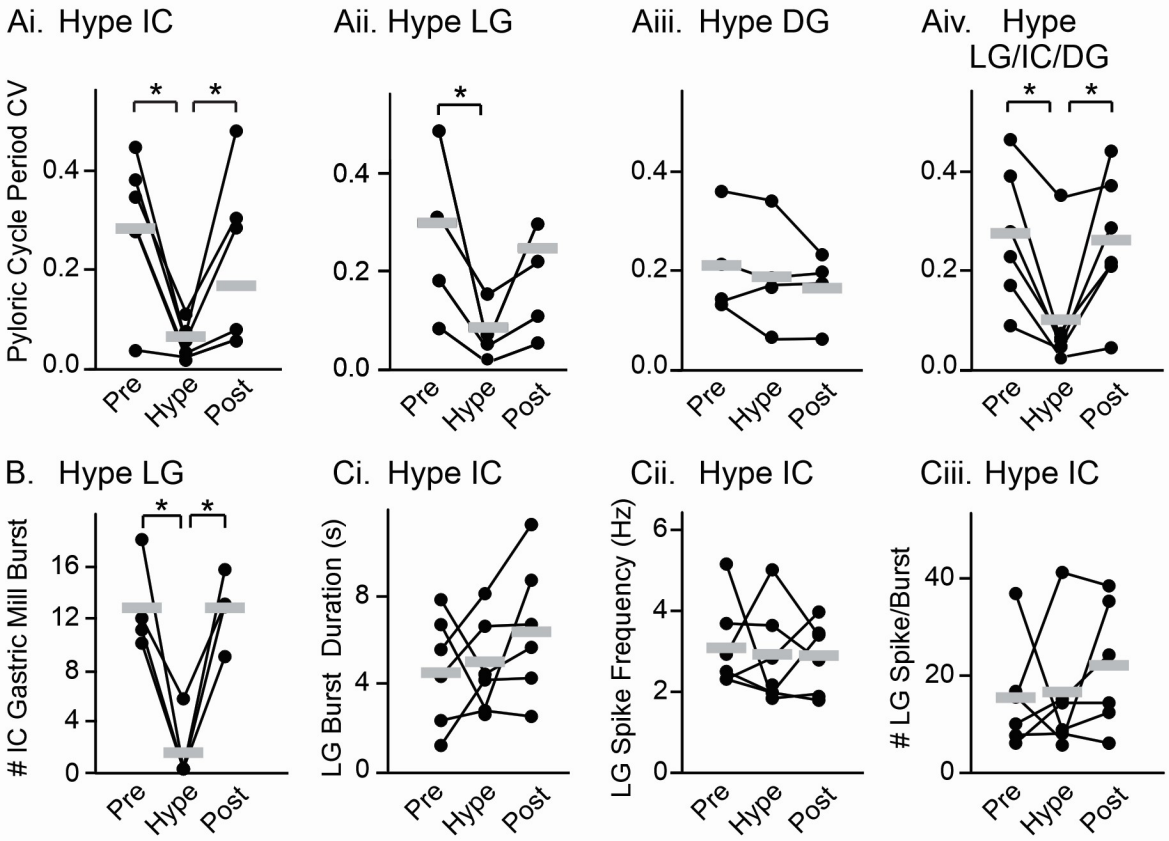

Figure 4
Gnanabharathi, Fahoum & Blitz

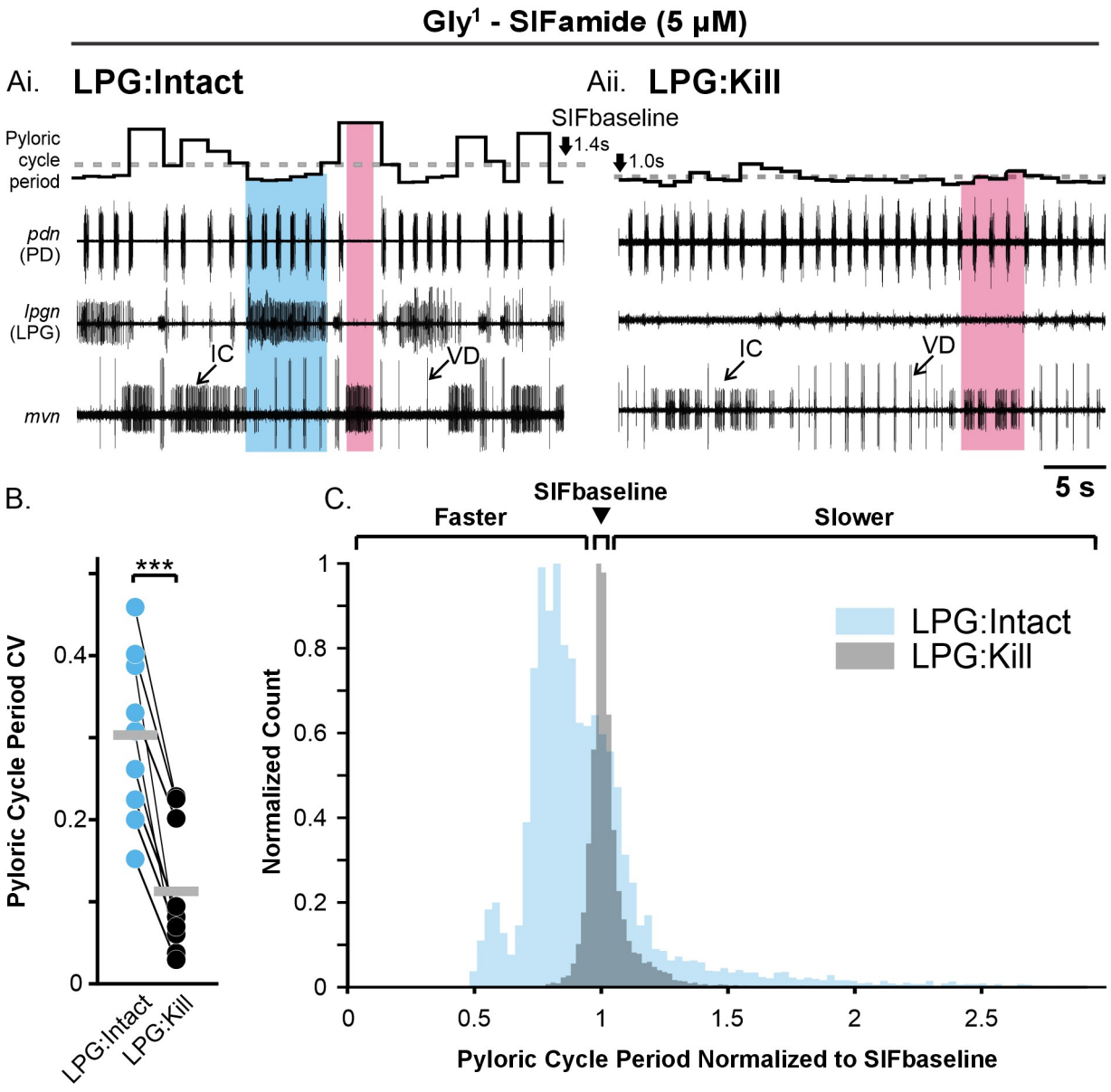

Figure 5
Gnanabharathi, Fahoum & Blitz

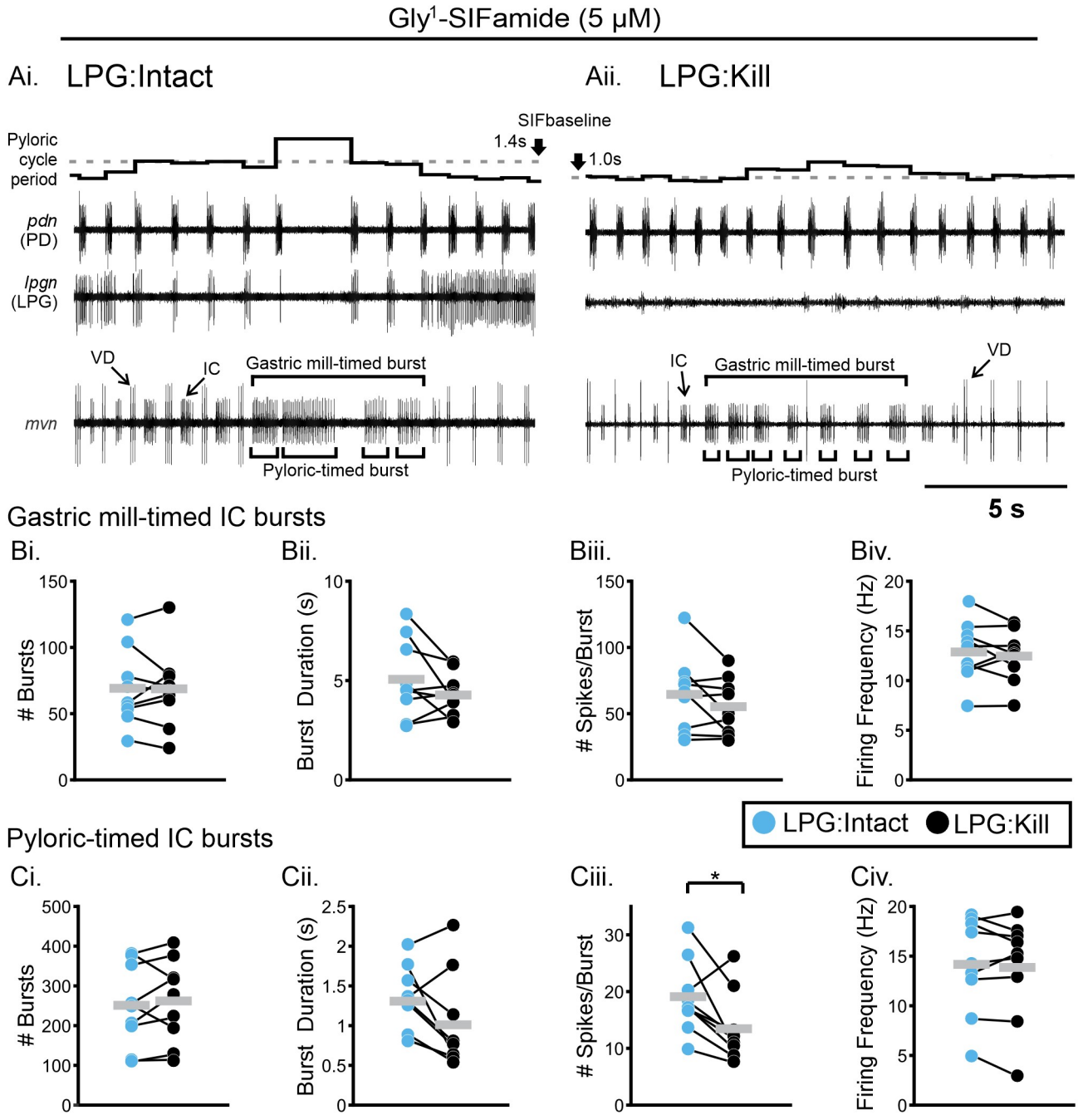

Figure 6
Gnanabharathi, Fahoum & Blitz

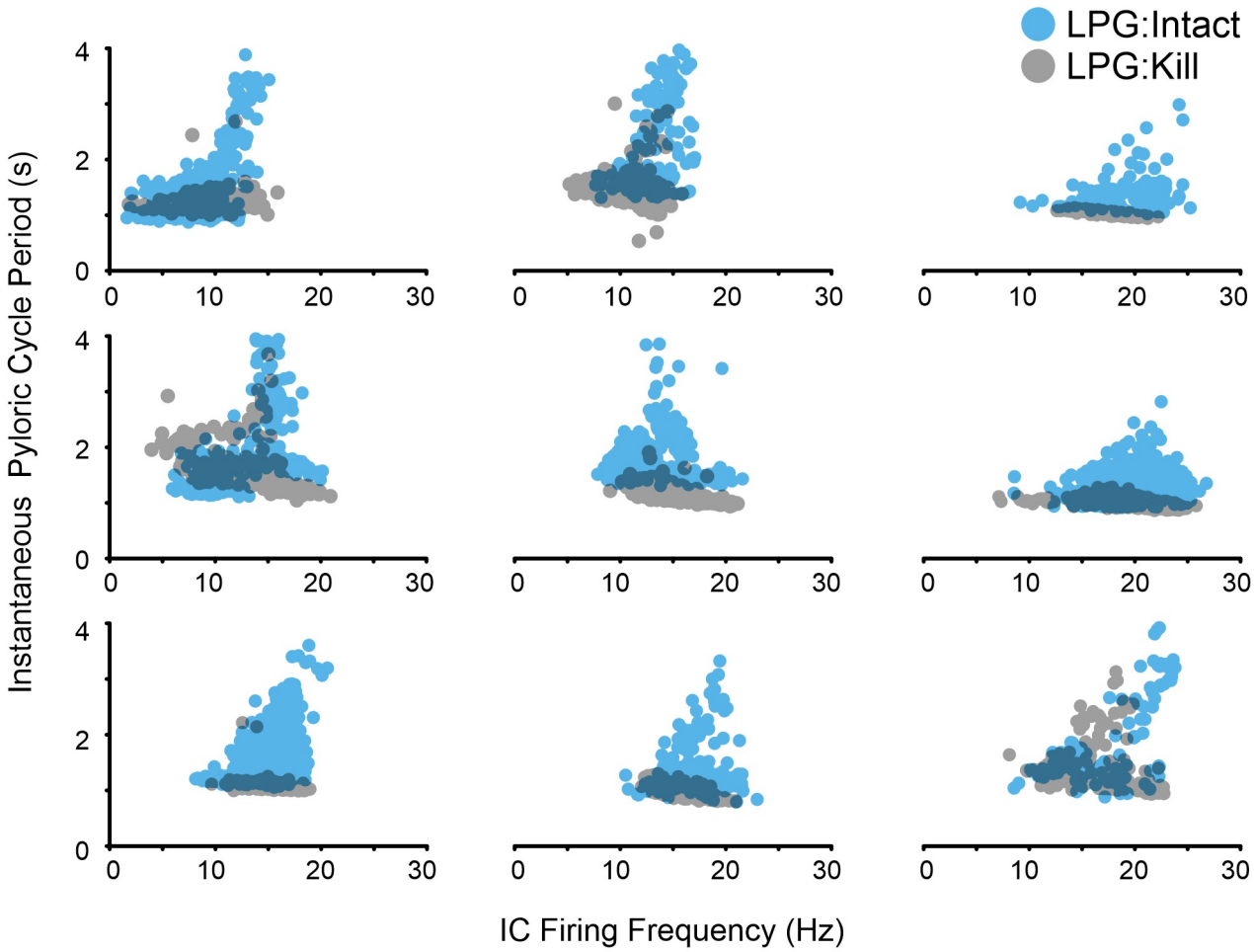

Figure 7
Gnanabharathi, Fahoum & Blitz

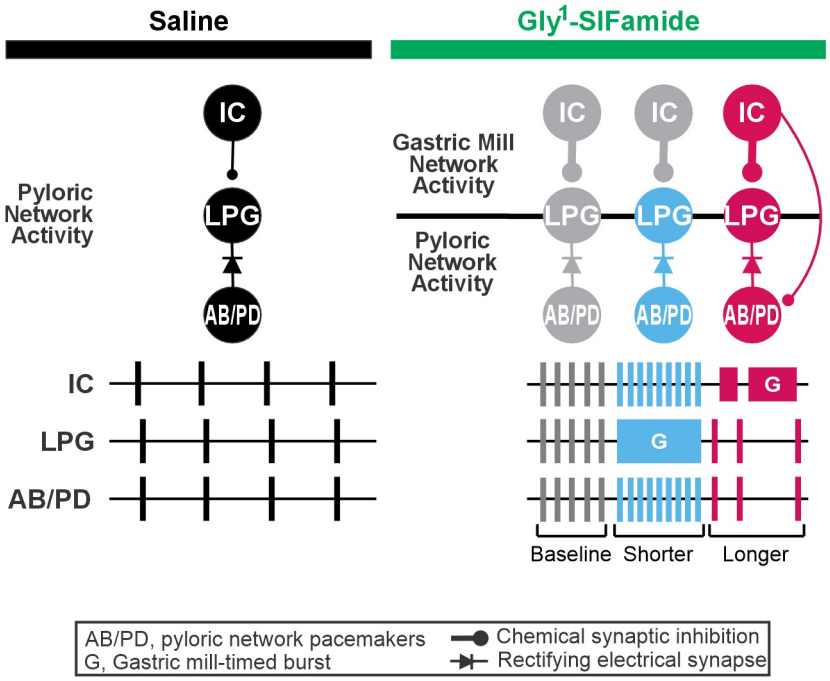

Figure 8
Gnanabharathi, Fahoum & Blitz